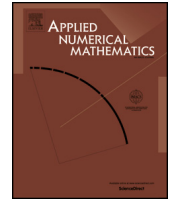


Contents lists available at ScienceDirect

Applied Numerical Mathematics

www.elsevier.com/locate/apnum

High-order numerical schemes based on difference potentials for 2D elliptic problems with material interfaces



Jason Albright^a, Yekaterina Epshteyn^{a,*}, Michael Medvinsky^b, Qing Xia^a

^a Department of Mathematics, The University of Utah, Salt Lake City, UT, 84112, United States

^b North Carolina State University, Raleigh, NC, 27695, United States

ARTICLE INFO

Article history:

Received 11 February 2016

Received in revised form 13 July 2016

Accepted 30 August 2016

Available online 8 September 2016

Keywords:

Boundary value problems

Piecewise-constant coefficients

High-order accuracy

Difference potentials

Boundary projections

Interface problems

Non-matching grids

Mixed-order

Parallel algorithms

Application to the simulation of the biological cell electroporation model

ABSTRACT

Numerical approximations and computational modeling of problems from Biology and Materials Science often deal with partial differential equations with varying coefficients and domains with irregular geometry. The challenge here is to design an efficient and accurate numerical method that can resolve properties of solutions in different domains/subdomains, while handling the arbitrary geometries of the domains. In this work, we consider 2D elliptic models with material interfaces and develop efficient high-order accurate methods based on Difference Potentials for such problems.

© 2016 IMACS. Published by Elsevier B.V. All rights reserved.

1. Introduction

Highly-accurate numerical methods (see [38], etc.) that can efficiently handle irregular geometry and interface problems (usually described by mathematical models that have input data and solutions with discontinuities/non-smoothness across the interfaces), are crucial for the resolution of different temporal and spatial scales of physical, biological, biomedical problems, and problems from material sciences (models for composite materials, fluids, chemotaxis models, biofilms), to name a few. The major challenge here is to design a robust method that accurately captures certain properties of the solutions in different domains/subdomains (different regularity of the solutions in the domains, positivity, etc.), while handling the arbitrary geometries of the domains/subdomains. Moreover, any standard numerical method designed for smooth solutions, in general and in any dimension, will fail to produce accurate solutions to interface problems due to discontinuities in the model's parameters/solutions.

There is extensive literature that addresses problems in domains with irregular geometries and interface problems. Among finite-difference based methods for such problems are the Immersed Boundary Method (IB) [25,26], etc., the Immersed Interface Method (IIM) [15–17], etc., the Ghost Fluid Method (GFM) [12,19,18], etc., the Matched Interface and Boundary Method (MIB) [45,43,46], etc., and the method based on the Integral Equations approach, [21], etc. Among the

* Corresponding author.

E-mail address: epshteyn@math.utah.edu (Y. Epshteyn).

finite-element methods for interface problems are [3,6,37,24,44,42,13], etc. These methods are sharp interface methods that have been employed to solve problems in science and engineering. For a detailed review of the subject the reader can consult [17]. However, in spite of great advances in the past 40 years in the numerical methods for problems in arbitrary domains and/or interface problems, it is still a challenge to develop efficient numerical algorithms that can deliver high-order accuracy in space (higher than second-order), and that can handle general boundary/interface conditions.

Therefore, we consider here an approach based on Difference Potentials Method (DPM) [31,32]. The DPM on its own, or in combination with other numerical methods, is an efficient technique for the numerical solution, as well as for the discrete modeling of interior and exterior boundary value problems in domains with arbitrary geometry (see for example, [31,32,20,33,39,22,34,35,7,8,10,1,2]). The main idea of DPM is to reduce uniquely solvable and well-posed boundary value problems to pseudo-differential boundary equations with projections. Methods based on Difference Potentials introduce computationally simple auxiliary domains (see for example [31,34,35,8,10,1,2,22], etc.). After that, the original domains are embedded into auxiliary domains (and the auxiliary domains are discretized using regular structured grids). Next, DPM constructs discrete pseudo-differential *Boundary Equations with Projections* to obtain the value of the solution at the points near the continuous boundary of the original domain (at the points of the discrete grid boundary which straddles the continuous boundary from the inside and outside of the domain). Using the reconstructed values of the solution at the discrete grid boundary, the approximation to the solution in each domain/subdomain is obtained through the discrete generalized Green's formula. *DPM offers geometric flexibility (without the use of unstructured meshes or "body-fitted" meshes), but does not require explicit knowledge of the fundamental solution. Furthermore, DPM is not limited to constant coefficient problems, does not involve singular integrals, and can handle general boundary and/or interface conditions.*

The major computational cost of methods based on the Difference Potentials approach reduces to several solutions of simple auxiliary problems on regular structured grids. Methods based on Difference Potentials preserve the underlying accuracy of the schemes being used for the space discretization of the continuous PDEs in each domain/subdomain and at the same time are not restricted by the type of the boundary or interface conditions (as long as the continuous problems are well-posed). Moreover, numerical schemes based on Difference Potentials are well-suited for the development of parallel algorithms (see [34,35,8], etc.). The reader can consult [31,32] and [28,29] for a detailed theoretical study of the methods based on Difference Potentials, and [31,32,11,20,33,39,36,22,5,34,35,7,8,10,1,2], etc. for the recent developments and applications of DPM.

In this work, we consider 2D elliptic models with material interfaces and develop efficient, high-order accurate (second-order and fourth-order) methods based on the Difference Potentials approach for such problems. This paper is an extension of the work in [10] to 2D models, and extension of the work in [34,35,8,9] to higher orders. The main contributions of the current work are 1) The development and validation of high-order methods based on Difference Potentials using central-difference discretization as the underlying approximation of the PDE (rather than compact schemes). Note that the employed central-difference stencils result in a multi-layer discrete grid boundary set for the BEP, and hence different BEP are constructed at the boundaries/interfaces in comparison to Difference Potentials schemes based on compact stencils (compact stencils [22,23] generate standard two-layer discrete grid boundary for BEP similar to the second-order central-difference stencil); 2) Consideration of the general interface conditions without assumptions of the continuity of the solution or/and continuity of the flux at the interface; 3) The conducted numerical experiments corroborate high-order accuracy and stability of the proposed numerical methods for interface problems with general interface conditions.

Let us also mention that a different example of an efficient and high-order accurate method, based on Difference Potentials and compact schemes for the Helmholtz equation in homogeneous media with the variable wave number in 2D, was recently developed and numerically tested in [22] and extended to the numerical simulation of the transmission and scattering of waves in [23].

The paper is organized as follows. First, in Section 2 we introduce the formulation of our problem. Next, to simplify the presentation of the ideas for the construction of DPM with different orders of accuracy, we construct DPM with second and with fourth-order accuracy together in Section 3.2 for elliptic type models in a single domain. In Section 4, we extend the second and the fourth-order DPM to interface/composite domain model problems. After that, in Section 5 we give a brief summary of the main steps of the proposed numerical algorithms. Finally, we illustrate the performance of the designed numerical algorithms based on Difference Potentials, as well as compare these algorithms with the Immersed Interface Method [15,4], Mayo's method [21,4] and recently developed Edge-Based Correction Finite Element Interface method (EBC-FEI) [13] in several numerical experiments in Section 6. We also present application of the developed methods based on Difference Potentials to the simulation of the linear static model of biological cell electropermeabilization (this model arises in Biological/Biomedical applications). Moreover, we illustrate in Section 6 that for DPM, the underlying numerical discretization (for example, numerical schemes with different orders of the approximation in different subdomains/domains), as well as meshes can be chosen totally independently for each subdomain/domain and the boundaries of the subdomains/interfaces do not need to conform/align with the grids. The constructed DPM based numerical algorithms are not restricted by the choice of boundary conditions, and the main computational complexity of the designed algorithms reduces to the several solutions of simple auxiliary problems on regular structured grids. Some concluding remarks are given in Section 7.

2. Elliptic problem with material interface

In this work we consider the interface/composite domain problem defined in some bounded domain $\Omega^0 \subset \mathbb{R}^2$:

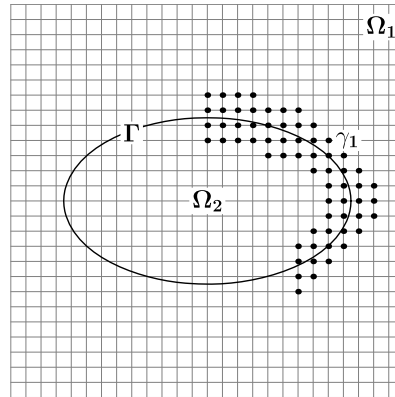


Fig. 1. Example of the composite domain: domains Ω_1 and Ω_2 separated by the interface Γ , and the example of the points in the discrete grid boundary set γ for the 9-point stencil of the fourth-order method. Auxiliary domain Ω^0 can be selected here to coincide with the boundary of the exterior domain Ω_1 .

$$L_{\Omega} u = \begin{cases} L_{\Omega_1} u_{\Omega_1} = f_1(x, y) & (x, y) \in \Omega_1 \\ L_{\Omega_2} u_{\Omega_2} = f_2(x, y) & (x, y) \in \Omega_2 \end{cases} \quad (2.1)$$

subject to the appropriate interface conditions:

$$\alpha_1 u_{\overline{\Omega_1}} \Big|_{\Gamma} - \alpha_2 u_{\overline{\Omega_2}} \Big|_{\Gamma} = \phi_1(x, y), \quad \beta_1 \frac{\partial u_{\overline{\Omega_1}}}{\partial n} \Big|_{\Gamma} - \beta_2 \frac{\partial u_{\overline{\Omega_2}}}{\partial n} \Big|_{\Gamma} = \phi_2(x, y) \quad (2.2)$$

and boundary conditions

$$l(u)|_{\partial\Omega_1} = \psi(x, y) \quad (2.3)$$

where $\Omega_1 \cup \Omega_2 = \Omega$ and $\Omega \subset \Omega^0$, see Fig. 1. Here, we assume L_{Ω_s} , $s \in \{1, 2\}$ are second-order linear elliptic differential operators of the form

$$L_{\Omega_s} u_{\Omega_s} \equiv \nabla \cdot (\lambda_s \nabla u_s) - \sigma_s u_s, \quad s \in \{1, 2\}. \quad (2.4)$$

The piecewise-constant coefficients $\lambda_s \geq 1$ and $\sigma_s \geq 0$ are defined in larger auxiliary subdomains $\Omega_s \subset \Omega_s^0$. The functions $f_s(x, y)$ are sufficiently smooth functions defined in each subdomain Ω_s and $\alpha_1, \alpha_2, \beta_1, \beta_2$ are coefficients (possibly variable coefficients). We assume that the continuous problem (2.1)–(2.3) is well-posed. Furthermore, we consider operators L_{Ω_s} which are well-defined on some larger auxiliary domain Ω_s^0 : we assume that for any sufficiently smooth function $f_s(x, y)$ on Ω_s^0 , the equation $L_{\Omega_s^0} u_{\Omega_s^0} = f_s(x, y)$ has a unique solution $u_{\Omega_s^0}$ on Ω_s^0 that satisfies the given boundary conditions on $\partial\Omega_s^0$.

Here and below, the index $s \in \{1, 2\}$ is introduced to distinguish between the subdomains.

3. Single domain

Our aim here is to construct high-order accurate numerical methods based on Difference Potentials that can handle general boundary and interface conditions for the elliptic interface problems (2.1)–(2.3). To simplify the presentation, we will first consider an elliptic problem defined in a single domain Ω :

$$L_{\Omega} u = f(x, y), \quad (x, y) \in \Omega \quad (3.1)$$

subject to the appropriate boundary conditions

$$l(u)|_{\Gamma} = \psi(x, y) \quad (3.2)$$

where $\Omega \subset \Omega^0$ and $\Gamma := \partial\Omega$, see Fig. 2, and then extend the proposed ideas in a direct way to the interface/composite domain problems (2.1)–(2.3) in Section 4.

Similar to the interface problem (2.1)–(2.3) we assume that L_{Ω} is the second-order linear elliptic differential operator of the form

$$L_{\Omega} u \equiv \nabla \cdot (\lambda \nabla u) - \sigma u. \quad (3.3)$$

The constant coefficients $\lambda \geq 1$ and $\sigma \geq 0$ are defined in a larger auxiliary subdomains $\Omega \subset \Omega^0$. The function $f(x, y)$ is a sufficiently smooth function defined in domain Ω . We assume that the continuous problem (3.1)–(3.2) is well-posed. Moreover, we consider here the operator L_{Ω} which is well-defined on some larger auxiliary domain: we assume that for any sufficiently smooth function $f(x, y)$ on Ω^0 , the equation $L_{\Omega^0} u = f(x, y)$ has a unique solution u_{Ω^0} on Ω^0 satisfying the given boundary conditions on $\partial\Omega^0$.

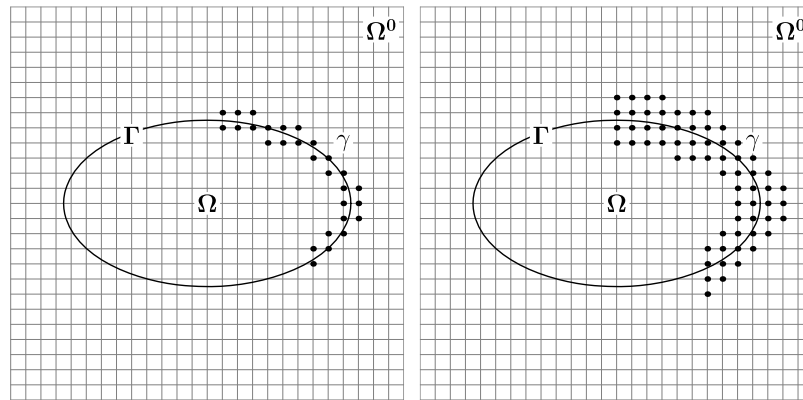


Fig. 2. Example of an auxiliary domain Ω^0 , original domain $\Omega \subset \Omega^0$, and the example of the points in the discrete grid boundary set γ for the 5-point stencil of the second-order method (left figure) and the example of the points in the discrete grid boundary set γ for the 9-point stencil of the fourth-order method (right figure).

3.1. Preliminaries to continuous potentials with projectors

The main focus of this paper is second-order linear elliptic equations of the form (3.1), (3.3). For the time being, we restrict our attention to constant coefficient elliptic operators (3.3). However, the main ideas of the method and definitions presented here extend in a straightforward way to elliptic models in heterogeneous media, see for example the recent work [10] – 1D settings, 2nd- and 4th-order methods; [9] – 2D settings, 2nd-order method for elliptic models in heterogeneous media, where methods based on Difference Potentials have been developed for elliptic problems in heterogeneous media in 1D and 2D space dimensions. It will be part of our future work to extend high-order methods developed here and in [1,2] to efficient high-order methods (higher than 2nd-order methods in space) for elliptic and parabolic interface models in heterogeneous media in 2D.

Recall here some mathematical preliminaries to continuous generalized Calderon’s potentials with projectors (see also [31,35,22], etc.). Difference Potentials (that will be employed here for construction of efficient and highly accurate algorithms for interface problems) are a discrete analogue of the continuous generalized Calderon’s potentials with projectors. *It is important to note that although this paper is focused on linear second-order elliptic problems, methods based on Difference Potentials are not limited to linear models or elliptic operators, [31,40,41].*

Consider here the second-order linear elliptic equations with constant coefficients of the form (3.1), (3.3), where $u(x, y) \in C_{\mu+2+\varepsilon, \bar{\Omega}}$, $\mu = 0, 1, \dots$, $0 < \varepsilon < 1$ is a solution to (3.1).

Recall, that the Cauchy data v_Γ for an arbitrary continuous piecewise smooth function $v(x, y)$ given on the boundary $\Gamma := \partial\Omega$ and in some of its neighborhoods are defined as the vector-function

$$v_\Gamma \equiv \mathbf{Tr}_\Gamma v = \left(v \Big|_\Gamma, \frac{\partial v}{\partial n} \Big|_\Gamma \right), \tag{3.4}$$

where $\frac{\partial}{\partial n}$ is the outward normal derivative relative to Ω , operator $\mathbf{Tr}_\Gamma v$ denotes the trace of $v(x, y)$ on the boundary Γ , and we assume that $v|_\Gamma \in C_{\mu+2+\varepsilon, \Gamma}$, $\frac{\partial v}{\partial n} \Big|_\Gamma \in C_{\mu+1+\varepsilon, \Gamma}$. Similarly to (3.4), denote u_Γ to be the Cauchy data of a solution u of (3.1). Now, if $G := G(x, y)$ is the fundamental solution of L_Ω , then recall classical Green’s formula for a solution $u(x, y)$ of (3.1):

$$u(x, y) = \int_\Gamma \left(u \frac{\partial G(x, y)}{\partial n} - \frac{\partial u}{\partial n} G(x, y) \right) ds + \iint_\Omega G(x, y) f(y) dy, \quad (x, y) \in \Omega \tag{3.5}$$

Recall, next, the definition of the *generalized potential of Calderon type* [30,31,40], see also [22]:

Definition 3.1. A generalized potential of Calderon type with vector density $\xi_\Gamma = (\xi_0, \xi_1)|_\Gamma$ is the convolution integral

$$\mathbf{P}_{\Omega\Gamma} \xi_\Gamma := \int_\Gamma \left(\xi_0 \frac{\partial G(x, y)}{\partial n} - \xi_1 G(x, y) \right) ds, \quad (x, y) \in \Omega \tag{3.6}$$

Review of some properties of continuous generalized potential of Calderon type, see [30,31,35,40], see also [22]:

1. For any density $\xi_\Gamma = (\xi_0, \xi_1)|_\Gamma$ with $\xi_0|_\Gamma \in C_{\mu+2+\varepsilon, \Gamma}$, $\xi_1|_\Gamma \in C_{\mu+1+\varepsilon, \Gamma}$, we have that

$$L_\Omega[\mathbf{P}_{\Omega\Gamma} \xi_\Gamma] = 0$$

2. In general, the trace of $\mathbf{P}_{\Omega\Gamma}\xi_\Gamma$ will not coincide with $\xi_\Gamma = (\xi_0, \xi_1)|_\Gamma : \mathbf{Tr}_\Gamma\mathbf{P}_{\Omega\Gamma}\xi_\Gamma \neq \xi_\Gamma$. However, if $u(x, y)$ is the solution of the homogeneous equation: $L_\Omega[u] = 0$ on Ω , and if it happens that the density $\xi_\Gamma \equiv \mathbf{Tr}_\Gamma u$ is the trace of that solution $u(x, y)$, then $\mathbf{P}_{\Omega\Gamma}\xi_\Gamma = u(x, y)$, $(x, y) \in \Omega$, and (3.6) becomes the classical Green’s formula for the solution of the homogeneous problem:

$$u(x, y) = \int_\Gamma \left(u \frac{\partial G(x, y)}{\partial n} - \frac{\partial u}{\partial n} G(x, y) \right) ds, \quad (x, y) \in \Omega$$

In other words, it can be shown that a given density function $\xi_\Gamma = (\xi_0, \xi_1)|_\Gamma$ with $\xi_0|_\Gamma \in C^{\mu+2+\epsilon, \Gamma}$, $\xi_1|_\Gamma \in C^{\mu+1+\epsilon, \Gamma}$ is the trace of a solution $u(x, y)$ to the homogeneous equation $L_\Omega[u] = 0$ on Ω : $\xi_\Gamma = \mathbf{Tr}_\Gamma u$, iff it satisfies the *homogeneous Boundary Equation with Projection (BEP)*:

$$\xi_\Gamma - \mathbf{P}_\Gamma \xi_\Gamma = 0 \tag{3.7}$$

Here, projection $\mathbf{P}_\Gamma \xi_\Gamma$ is the Calderon projection defined as the trace on Γ of the potential $\mathbf{P}_{\Omega\Gamma}\xi_\Gamma$:

$$\mathbf{P}_\Gamma \xi_\Gamma := \mathbf{Tr}_\Gamma \mathbf{P}_{\Omega\Gamma} \xi_\Gamma. \tag{3.8}$$

Note, that it can be shown that the operator $\mathbf{P}_\Gamma \xi_\Gamma$ is an actual projection operator: $\mathbf{P}_\Gamma \xi_\Gamma = \mathbf{P}_\Gamma^2 \xi_\Gamma$.

3. Similarly to (3.7), a given density function $\xi_\Gamma = (\xi_0, \xi_1)|_\Gamma$ is the trace of a solution $u(x, y)$ to the inhomogeneous equation $L_\Omega[u] = f$ on Ω : $\xi_\Gamma = \mathbf{Tr}_\Gamma u$, iff it satisfies the *inhomogeneous Boundary Equation with Projection (BEP)*:

$$\xi_\Gamma - \mathbf{P}_\Gamma \xi_\Gamma = \mathbf{Tr}_\Gamma Gf. \tag{3.9}$$

Here, G denotes the Green’s operator, the inverse $Gf \equiv \iint_\Omega G(x, y)f(y)dy$, see classical Green’s formula above (3.5).

Finally, after some density ξ_Γ is obtained from (BEP) (3.9), the solution $u(x, y)$ on Ω is obtained from the *Generalized Green’s Formula*:

$$u = \mathbf{P}_{\Omega\Gamma}\xi_\Gamma + Gf, \tag{3.10}$$

where $\xi_\Gamma = \mathbf{Tr}_\Gamma u$.

(Similarly, in the homogeneous case: $u = \mathbf{P}_{\Omega\Gamma}\xi_\Gamma$.)

4. Note, that inhomogeneous (BEP) (3.9) has multiple solutions ξ_Γ since the equation $L_\Omega[u] = f$ on Ω has multiple solutions u on Ω (similarly, the homogeneous (BEP) (3.7) alone has multiple solutions ξ_Γ since the equation $L_\Omega[u] = 0$ on Ω has multiple solutions u on Ω). To find a unique solution u one must impose appropriate boundary conditions (3.2). Hence, one has to solve (BEP) together with the boundary conditions to find a unique density ξ_Γ :

$$\xi_\Gamma - \mathbf{P}_\Gamma \xi_\Gamma = \mathbf{Tr}_\Gamma Gf, \tag{3.11}$$

$$l(\mathbf{P}_{\Omega\Gamma}\xi_\Gamma + Gf)|_\Gamma = \psi(x, y), \tag{3.12}$$

(similarly, in the homogeneous case, to find a unique density ξ_Γ , one has to solve $\xi_\Gamma - \mathbf{P}_\Gamma \xi_\Gamma = 0$ and $l(\mathbf{P}_{\Omega\Gamma}\xi_\Gamma)|_\Gamma = \psi(x, y)$).

5. For the detailed theory and more properties of the generalized Calderon’s potentials (including construction of the method for nonlinear problems) the reader can consult [30,31,40,41], see also [35,22], etc.

3.2. High-order methods based on difference potentials

The current work is an extension of the work started in 1D settings in [10] to the 2D elliptic models. For time being we restrict our attention here to models with piecewise-constant coefficients. However, the construction of the methods presented below allows for a straightforward extension to models in heterogeneous media, which will be part of our future research. In this work, the choices of the second-order discretization (3.16) and the fourth-order discretization (3.17) below were considered for the purpose of the efficient illustration and implementation of the ideas, as well as for the ease of the future extension to models in heterogeneous media. However, the approach presented here based on Difference Potentials is general, and can be similarly used with any suitable underlying high-order discretization of the given continuous model: DPM is the method of building a discrete approximation to the continuous generalized Calderon’s potentials, (3.6) and to the continuous Boundary Equations with Projections (BEP), (3.11)–(3.12), (3.10) (see [31] for the detailed theoretical foundation of DPM).

Similar to [10], we will illustrate our ideas below by constructing the second and the fourth-order schemes together, and will only comment on the differences between them.

Introduction of the Auxiliary Domain: Place the original domain Ω in the computationally simple auxiliary domain $\Omega^0 \subset \mathbb{R}^2$ that we will choose to be a square. Next, introduce a Cartesian mesh for Ω^0 , with points $x_j = j\Delta x$, $y_k = k\Delta y$, $(k, j = 0, \pm 1, \dots)$. Let us assume for simplicity that $h := \Delta x = \Delta y$.

Define a finite-difference stencil $N_{j,k}^\kappa := N_{j,k}^5$ or $N_{j,k}^\kappa := N_{j,k}^9$ with its center placed at (x_j, y_k) , to be a 5-point central finite-difference stencil of the second-order method, or a 9-point central finite-difference stencil of the fourth-order method, respectively, see Fig. 3:

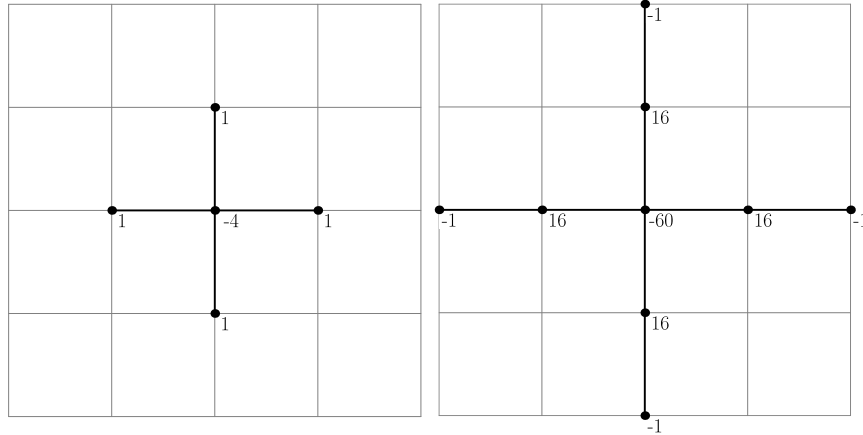


Fig. 3. Example (a sketch) of the 5-point stencil for the second-order scheme (3.13) (left figure) and example (a sketch) of the 9-point stencil for the fourth-order scheme (3.14) (right figure).

$$N_{j,k}^\kappa := \{(x_j, y_k), (x_{j\pm 1}, y_k), (x_j, y_{k\pm 1})\}, \quad \kappa = 5, \text{ or} \tag{3.13}$$

$$N_{j,k}^\kappa := \{(x_j, y_k), (x_{j\pm 1}, y_k), (x_j, y_{k\pm 1}), (x_{j\pm 2}, y_k), (x_j, y_{k\pm 2})\}, \quad \kappa = 9 \tag{3.14}$$

Next, introduce the point sets M^0 (the set of all mesh nodes (x_j, y_k) that belong to the interior of the auxiliary domain Ω^0), $M^+ := M^0 \cap \Omega$ (the set of all the mesh nodes (x_j, y_k) that belong to the interior of the original domain Ω), and $M^- := M^0 \setminus M^+$ (the set of all the mesh nodes (x_j, y_k) that are inside of the auxiliary domain Ω^0 but belong to the exterior of the original domain Ω). Define $N^+ := \{\bigcup_{j,k} N_{j,k}^\kappa | (x_j, y_k) \in M^+\}$ (the set of all points covered by the stencil $N_{j,k}^\kappa$ when the center point (x_j, y_k) of the stencil goes through all the points of the set $M^+ \subset \Omega$). Similarly define $N^- := \{\bigcup_{j,k} N_{j,k}^\kappa | (x_j, y_k) \in M^-\}$ (the set of all points covered by the stencil $N_{j,k}^\kappa$ when center point (x_j, y_k) of the stencil goes through all the points of the set M^-).

Now, we can introduce $\gamma := N^+ \cap N^-$. The set γ is called the *discrete grid boundary*. The mesh nodes from set γ straddle the boundary $\Gamma \equiv \partial\Omega$. Finally, define $N^0 := \{\bigcup_{j,k} N_{j,k}^\kappa | (x_j, y_k) \in M^0\} \subseteq \overline{\Omega^0}$.

Remark. From here and below κ either takes the value 5 (if the 5-point stencil is used to construct the second-order method), or 9 (if the 9-point stencil is used to construct the fourth-order method).

The sets $N^0, M^0, N^+, N^-, M^+, M^-, \gamma$ will be used to develop high-order methods in 2D based on the Difference Potentials idea.

Construction of the Difference Equations: The discrete version of the problem (3.1) is to find $u_{j,k}, (x_j, y_k) \in N^+$ such that

$$L_h[u_{j,k}] = f_{j,k}, \quad (x_j, y_k) \in M^+ \tag{3.15}$$

The discrete system of equations (3.15) is obtained here by discretizing (3.1) with the second-order 5-point central finite difference scheme (3.16) (if the second-order accuracy is desired), or with the fourth-order 9-point central finite difference scheme in space (3.17) (if the fourth-order accuracy is needed). Here and below, by L_h we assume the discrete linear operator obtained using either the second-order approximation to (3.1), or the fourth-order approximation to (3.1), and by $f_{j,k}$ a discrete right-hand side.

Second-Order Scheme:

$$L_h[u_{j,k}] := \lambda \frac{u_{j+1,k} - 2u_{j,k} + u_{j-1,k}}{h^2} + \lambda \frac{u_{j,k+1} - 2u_{j,k} + u_{j,k-1}}{h^2} - \sigma u_{j,k}. \tag{3.16}$$

The right-hand side in the discrete system (3.15) is $f_{j,k} := f(x_j, y_k)$ for the second-order method.

Fourth-Order Scheme:

$$L_h[u_{j,k}] := \lambda \frac{-u_{j+2,k} + 16u_{j+1,k} - 30u_{j,k} + 16u_{j-1,k} - u_{j-2,k}}{12h^2} + \lambda \frac{-u_{j,k+2} + 16u_{j,k+1} - 30u_{j,k} + 16u_{j,k-1} - u_{j,k-2}}{12h^2} - \sigma u_{j,k} \tag{3.17}$$

Again, the right-hand side in the discrete system (3.15) in case of fourth-order discretization (3.17) is $f_{j,k} := f(x_j, y_k)$.

Remark. The standard second-order and fourth-order schemes (3.16)–(3.17) above are employed here as the underlying discretization of the continuous equation (3.1) similar to the 1D work, [10].

In general, the linear system of difference equations (3.15) will have multiple solutions as we did not enforce any boundary conditions. Once we complete the discrete system (3.15) with the appropriate discrete boundary conditions, the method will result in an accurate approximation of the continuous model (3.1)–(3.2) in domain Ω . To do so efficiently, we will construct numerical algorithms based on the idea of the Difference Potentials.

General Discrete Auxiliary Problem: Some of the important steps of DPM are the introduction of the auxiliary problem, which we will denote as (AP), as well as definitions of the particular solution and Difference Potentials. Let us recall these definitions below (see also [31,10,9], etc.).

Definition 3.2. The problem of solving (3.18)–(3.19) is referred to as the discrete auxiliary problem (AP): For the given grid function $q, (x_j, y_k) \in M^0$, find the solution $v, (x_j, y_k) \in N^0$ of the discrete (AP) such that it satisfies the following system of equations:

$$L_h[v_{j,k}] = q_{j,k}, \quad (x_j, y_k) \in M^0, \quad (3.18)$$

$$v_{j,k} = 0, \quad (x_j, y_k) \in N^0 \setminus M^0. \quad (3.19)$$

Here, L_h is the same linear discrete operator as in (3.15), but now it is defined on the larger auxiliary domain $\overline{\Omega^0}$ (note that, we assumed before in Section 3 that the continuous operator on the left-hand side of the equation (3.1) is well-defined on the entire domain $\overline{\Omega^0}$). It is applied in (3.18) to the function $v, (x_j, y_k) \in N^0$. We remark that under the above assumptions on the continuous model, the (AP) (3.18)–(3.19) is well-defined for any right-hand side function q on M^0 : it has a unique solution v on N^0 . In this work we supplemented the discrete (AP) (3.18) by the zero boundary conditions (3.19). In general, the boundary conditions for (AP) are selected to guarantee that the discrete system $L_h[v_{j,k}] = q_{j,k}$ has a unique solution v on N^0 for any discrete right-hand side function q on M^0 .

Remark. The solution of the (AP) (3.18)–(3.19) defines a discrete Green's operator G^h (or the inverse operator to L_h). Although the choice of boundary conditions (3.19) will affect the operator G^h , and hence the difference potentials and the projections defined below, it will not affect the final approximate solution to (3.1)–(3.2), as long as the (AP) is uniquely solvable and well-posed.

Construction of a Particular Solution: Let us denote by $u_{j,k} := G^h f_{j,k}, (x_j, y_k) \in N^+$ the particular solution of the discrete problem (3.15), which we will construct as the solution (restricted to set N^+) of the auxiliary problem (AP) (3.18)–(3.19) of the following form:

$$L_h[u_{j,k}] = \begin{cases} f_{j,k}, & (x_j, y_k) \in M^+, \\ 0, & (x_j, y_k) \in M^-, \end{cases} \quad (3.20)$$

$$u_{j,k} = 0, \quad (x_j, y_k) \in N^0 \setminus M^0 \quad (3.21)$$

Difference Potential: We now introduce a linear space V_γ of all the grid functions denoted by v_γ defined on γ , [31,10], etc. We will extend the value v_γ by zero to other points of the grid N^0 .

Definition 3.3. The Difference Potential with any given density $v_\gamma \in V_\gamma$ is the grid function $u_{j,k} := \mathbf{P}_{N^+} v_\gamma$, defined on N^+ , and coincides on N^+ with the solution $u_{j,k}$ of the auxiliary problem (AP) (3.18)–(3.19) of the following form:

$$L_h[u_{j,k}] = \begin{cases} 0, & (x_j, y_k) \in M^+, \\ L_h[v_\gamma], & (x_j, y_k) \in M^-, \end{cases} \quad (3.22)$$

$$u_{j,k} = 0, \quad (x_j, y_k) \in N^0 \setminus M^0 \quad (3.23)$$

The Difference Potential is the discrete inverse operator. Here, \mathbf{P}_{N^+} denotes the operator which constructs the difference potential $u_{j,k} = \mathbf{P}_{N^+} v_\gamma$ from the given density $v_\gamma \in V_\gamma$. The operator \mathbf{P}_{N^+} is the linear operator of the density v_γ : $u_m = \sum_{l \in \gamma} A_{lm} v_l$, where $m \equiv (j, k)$ is the index of the grid point in the set N^+ and l is the index of the grid point in the set γ . Here, value u_m is the value of the difference potential $\mathbf{P}_{N^+} v_\gamma$ at the grid point with an index m : $u_m = \mathbf{P}_{N^+} v_\gamma|_m$ and coefficients $\{A_{lm}\}$ are the coefficients of the difference potentials operator. The coefficients $\{A_{lm}\}$ can be computed by solving simple auxiliary problems (AP) (3.22)–(3.23) (or by constructing a Difference Potential operator) with the appropriate density v_γ defined at the points $(x_j, y_k) \in \gamma$.

Next, similarly to [31,10], etc., we can define another operator $\mathbf{P}_\gamma : V_\gamma \rightarrow V_\gamma$ that is defined as the trace (or restriction/projection) of the Difference Potential $\mathbf{P}_{N^+} v_\gamma$ on the grid boundary γ :

$$\mathbf{P}_\gamma v_\gamma := \text{Tr}_\gamma(\mathbf{P}_{N+\gamma} v_\gamma) = (\mathbf{P}_{N+\gamma} v_\gamma)|_\gamma \tag{3.24}$$

We will now formulate the crucial theorem of DPM (see, for example [31,10], etc.).

Theorem 3.4. *Density u_γ is the trace of some solution u to the Difference Equations (3.15): $u_\gamma \equiv \text{Tr}_\gamma u$, if and only if, the following equality holds*

$$u_\gamma = \mathbf{P}_\gamma u_\gamma + G^h f_\gamma, \tag{3.25}$$

where $G^h f_\gamma := \text{Tr}_\gamma(G^h f)$ is the trace (or restriction) of the particular solution $G^h f, (x_j, y_k) \in N^+$ constructed in (3.20)–(3.21) on the grid boundary γ .

Proof. The proof follows closely the general argument from [31] and can be found, for example, in [10] (the extension to higher-dimension is straightforward). \square

Remark.

1. Note that the difference potential $\mathbf{P}_{N+\gamma} u_\gamma$ is the solution to the homogeneous difference equation $L_h[u_{j,k}] = 0, (x_j, y_k) \in M^+$, and is uniquely defined once we know the value of the density u_γ at the points of the boundary γ .
2. Note, also that the difference potential $\mathbf{P}_{N+\gamma} u_\gamma$ is the discrete approximation to the generalized potentials of the Calderon’s type $\mathbf{P}_{\Omega\Gamma\xi_\Gamma}$ (3.6): $\mathbf{P}_{N+\gamma} u_\gamma \approx \mathbf{P}_{\Omega\Gamma\xi_\Gamma}$. Due to the construction of the extension operators (3.27) and (3.28), single-valued density u_γ incorporates the information about the Cauchy data $\xi_\Gamma = (\xi_0, \xi_1)$ of the continuous solution $u(x, y)$.
3. Moreover, note that the density u_γ has to satisfy *discrete Boundary Equations* $u_\gamma - \mathbf{P}_\gamma u_\gamma = G^h f_\gamma$ in order to be a trace of the solution to the difference equation $L_h[u_{j,k}] = f_{j,k}, (x_j, y_k) \in M^+$.
4. The discrete boundary equations with projection $u_\gamma - \mathbf{P}_\gamma u_\gamma = G^h f_\gamma$, (3.25) is the discrete analogue of the continuous boundary equations with projection $\xi_\Gamma - \mathbf{P}_\Gamma \xi_\Gamma = \mathbf{Tr}_\Gamma Gf$, (3.9).

Coupling of Boundary Equations with Boundary Conditions: The discrete *Boundary Equations with Projections* (3.25) which can be rewritten in a slightly different form as:

$$(\mathbf{I} - \mathbf{P}_\gamma)u_\gamma = G^h f_\gamma, \tag{3.26}$$

is the linear system of equations for the unknown density u_γ . Here, \mathbf{I} is the identity operator, \mathbf{P}_γ is the projection operator, and the known right-hand side $G^h f_\gamma$ is the trace of the particular solution (3.20) on the discrete grid boundary γ .

The above system of discrete *Boundary Equations* (3.26) will have multiple solutions without boundary conditions (3.2), since it is equivalent to the difference equations $L_h[u_{j,k}] = f_{j,k}, (x_j, y_k) \in M^+$. We need to supplement it by the boundary conditions (3.2) to construct the unique density $u_\gamma \approx u(x, y)|_\gamma$, where $u(x, y)$ is the solution to the continuous model (3.1)–(3.2).

Thus, we will consider the following approach to solve for the unknown density u_γ from the discrete *Boundary Equations* (3.26). One can represent the unknown densities u_γ through the values of the continuous solution and its gradients at the boundary of the domain with the desired accuracy: *in other words, one can define the smooth extension operator for the solution of (3.1), from the continuous boundary $\Gamma = \partial\Omega$ to the discrete boundary γ . Note that the extension operator (the way it is constructed below) depends only on the properties of the given model at the continuous boundary Γ .*

For example, in case of 3 terms, the extension operator is:

$$\pi_{\gamma\Gamma}[u_\Gamma] \equiv u_{j,k} := u|_\Gamma + d \frac{\partial u}{\partial n} \Big|_\Gamma + \frac{d^2}{2!} \frac{\partial^2 u}{\partial n^2} \Big|_\Gamma, \quad (x_j, y_k) \in \gamma, \tag{3.27}$$

where $\pi_{\gamma\Gamma}[u_\Gamma]$ defines the smooth extension operator of Cauchy data u_Γ from the continuous boundary Γ to the discrete boundary γ , d denotes the signed distance from the point $(x_j, y_k) \in \gamma$ to the nearest boundary point on the continuous boundary Γ of the domain Ω (the signed length of the shortest normal from the point $(x_j, y_k) \in \gamma$ to the point on the continuous boundary Γ of the domain Ω). We take it either with sign “+” (if the point $(x_j, y_k) \in \gamma$ is outside of the domain Ω), or with sign “−” (if the point $(x_j, y_k) \in \gamma$ is inside the domain Ω). The choice of a 3 term extension operator (3.27) is sufficient for the second-order method based on Difference Potentials (see numerical tests (even with challenging geometry) in Section 6, as well as [31,10], etc.).

For example, in case of 5 terms, the extension operator is:

$$\pi_{\gamma\Gamma}[u_\Gamma] \equiv u_{j,k} := u|_\Gamma + d \frac{\partial u}{\partial n} \Big|_\Gamma + \frac{d^2}{2!} \frac{\partial^2 u}{\partial n^2} \Big|_\Gamma + \frac{d^3}{3!} \frac{\partial^3 u}{\partial n^3} \Big|_\Gamma + \frac{d^4}{4!} \frac{\partial^4 u}{\partial n^4} \Big|_\Gamma, \quad (x_j, y_k) \in \gamma, \tag{3.28}$$

again, as in (3.27), $\pi_{\gamma\Gamma}[u_\Gamma]$ defines the smooth extension operator of Cauchy data u_Γ from the continuous boundary Γ to the discrete boundary γ , d denotes the signed distance from the point $(x_j, y_k) \in \gamma$ to the nearest boundary point on the continuous boundary Γ of the domain Ω . As before, we take it either with sign “+” (if the point $(x_j, y_k) \in \gamma$ is outside

of the domain Ω), or with sign “–” (if the point $(x_j, y_k) \in \gamma$ is inside the domain Ω). The choice of a 5 term extension operator (3.28) is sufficient for the fourth-order method based on Difference Potentials (see Section 6, [10], etc.).

For any sufficiently smooth single-valued periodic function $g(\vartheta)$ on Γ with a period $|\Gamma|$, assume that the sequence

$$\varepsilon_{\mathcal{N}^0, \mathcal{N}^1} = \min_{c_v^0, c_v^1} \int_{\Gamma} \left(|g(\vartheta) - \sum_{v=0}^{\mathcal{N}^0} c_v^0 \phi_v^0(\vartheta)|^2 + |g'(\vartheta) - \sum_{v=0}^{\mathcal{N}^1} c_v^1 \phi_v^1(\vartheta)|^2 \right) d\vartheta \quad (3.29)$$

tends to zero with increasing $(\mathcal{N}^0, \mathcal{N}^1) : \lim \varepsilon_{\mathcal{N}^0, \mathcal{N}^1} = 0$ as $\mathcal{N}^0 \rightarrow \infty, \mathcal{N}^1 \rightarrow \infty$. Here, ϑ can be thought as the arc length along Γ , and $|\Gamma|$ is the length of the boundary. We selected arc length ϑ at this point only for definiteness. Other parameters along Γ are used in the numerical examples (polar coordinates for the circle and elliptical coordinates for the ellipse), see Section 6 and the brief discussion below. Note that, very similar construction of the extension operator and DPM applies to models in domains with general curvilinear boundaries without any special assumption on the shape of Γ (the difference can be in the choice of the parametrization/local coordinates for the boundary of the domain), [34,35,8].

Therefore, to discretize the elements $\xi|_{\Gamma} = \mathbf{Tr}\xi \equiv \left(\xi(\vartheta)|_{\Gamma}, \frac{\partial \xi}{\partial n}(\vartheta)|_{\Gamma} \right)$ from the space of Cauchy data, one can use the approximate equalities:

$$\tilde{\xi}_{\Gamma} = \sum_{v=0}^{\mathcal{N}^0} c_v^0 \Phi_v^0(\vartheta) + \sum_{v=0}^{\mathcal{N}^1} c_v^1 \Phi_v^1(\vartheta), \quad \tilde{\xi}_{\Gamma} \approx \xi_{\Gamma} \quad (3.30)$$

where $\Phi_v^0 = (\phi_v^0, 0)$ and $\Phi_v^1 = (0, \phi_v^1)$ are the set of basis functions to represent the Cauchy data on the boundary of the domain Γ and (c_v^0, c_v^1) with $(v = 0, 1, \dots, \mathcal{N}^0, v = 0, 1, \dots, \mathcal{N}^1)$ are the unknown numerical coefficients to be determined.

Remark. For smooth Cauchy data, it is expected that a relatively small number $(\mathcal{N}^0, \mathcal{N}^1)$ of basis functions are required to approximate the Cauchy data of the unknown solution, due to the rapid convergence of the expansions (3.30). Hence, in practice, we use a relatively small number of basis functions in (3.30), which leads to a very efficient numerical algorithm based on Difference Potentials approach, see Section 6 for a numerical illustration of the method.

In the case of the Dirichlet boundary condition in (3.1)–(3.2), $u(\vartheta)|_{\Gamma}$ is known, and hence, the coefficients c_v^0 above in (3.30) are given as the data which can be determined as the minimization of $\int_{\Gamma} |u(\vartheta) - \sum_{v=0}^{\mathcal{N}^0} c_v^0 \phi_v^0|^2 d\vartheta$. For other boundary value problems (3.1), the procedure is similar to the case presented for Dirichlet data. For example, in the case of Neumann boundary condition in (3.2), the coefficients c_v^1 in (3.30) are known and again found as the minimization of $\int_{\Gamma} |\frac{\partial u}{\partial n}(\vartheta) - \sum_{v=0}^{\mathcal{N}^1} c_v^1 \phi_v^1|^2 d\vartheta$.

1. Example of the construction of the extension operator in case of circular domains and polar angle θ as the parametrization parameter, $\vartheta \equiv \theta$: The elliptic equation in (3.1) can be rewritten in standard polar coordinates (r, θ) as:

$$\lambda \left(\frac{\partial^2 u}{\partial r^2} + \frac{1}{r} \frac{\partial u}{\partial r} + \frac{1}{r^2} \frac{\partial^2 u}{\partial \theta^2} \right) - \sigma u = f \quad (3.31)$$

The coordinate r corresponds to the distance from the origin along the normal direction \mathbf{n} to the circular interface Γ . Hence, extension operators (3.27)–(3.28) are equivalent to:

$$\pi_{\gamma\Gamma}[u_{\Gamma}] \equiv u_{j,k}(r_0, \theta) = u|_{\Gamma} + d \frac{\partial u}{\partial r}|_{\Gamma} + \frac{d^2}{2} \frac{\partial^2 u}{\partial r^2}|_{\Gamma} \quad (3.32)$$

and

$$\pi_{\gamma\Gamma}[u_{\Gamma}] \equiv u_{j,k}(r_0, \theta) = u|_{\Gamma} + d \frac{\partial u}{\partial r}|_{\Gamma} + \frac{d^2}{2!} \frac{\partial^2 u}{\partial r^2}|_{\Gamma} + \frac{d^3}{3!} \frac{\partial^3 u}{\partial r^3}|_{\Gamma} + \frac{d^4}{4!} \frac{\partial^4 u}{\partial r^4}|_{\Gamma}, \quad (3.33)$$

where, as before, $d = r - r_0$ denotes the signed distance from a grid point $(x_j, y_k) \in \gamma$ on the radius r , to the nearest point $(x, y) \in \Gamma$ on the original circle corresponding to the radius r_0 . The higher-order derivatives $\frac{\partial^e u}{\partial r^e}$, $e = 2, 3, \dots$ on Γ in (3.32)–(3.33) can be obtained through the Cauchy data $(u(\theta)|_{\Gamma}, \frac{\partial u}{\partial r}(\theta)|_{\Gamma})$, and the consecutive differentiation of the governing differential equation (3.31) with respect to r as illustrated below:

$$\frac{\partial^2 u}{\partial r^2} = \frac{f + \sigma u}{\lambda} - \frac{1}{r^2} \frac{\partial^2 u}{\partial \theta^2} - \frac{1}{r} \frac{\partial u}{\partial r}. \quad (3.34)$$

The expression (3.34) for $\frac{\partial^2 u}{\partial r^2}$ is used in the 3-term extension operator (3.32) in the second-order method, and is used in the 5-term extension operator (3.33) in the fourth-order method.

Similarly, in the 5-term extension operator (3.33), terms $\frac{\partial^3 u}{\partial r^3}$ and $\frac{\partial^4 u}{\partial r^4}$ are replaced by the following expressions:

$$\frac{\partial^3 u}{\partial r^3} = -\frac{1}{r} \frac{f + \sigma u}{\lambda} + \frac{3}{r^3} \frac{\partial^2 u}{\partial \theta^2} + \frac{1}{\lambda} \frac{\partial f}{\partial r} + \left(\frac{\sigma}{\lambda} + \frac{2}{r^2} \right) \frac{\partial u}{\partial r} - \frac{1}{r^2} \frac{\partial^2}{\partial \theta^2} \frac{\partial u}{\partial r} \quad (3.35)$$

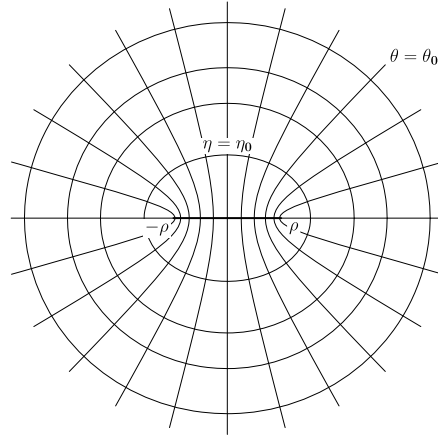


Fig. 4. Sketch of the elliptical coordinate system: distance from the center of the ellipse to either foci – ρ ; isoline – η ; elliptical angle – θ .

$$\frac{\partial^4 u}{\partial r^4} = \left(\frac{\sigma}{\lambda} + \frac{3}{r^2}\right) \frac{f + \sigma u}{\lambda} - \left(\frac{11}{r^4} + \frac{2\sigma}{r^2 \lambda}\right) \frac{\partial^2 u}{\partial \theta^2} + \frac{1}{r^4} \frac{\partial^4 u}{\partial \theta^4} \tag{3.36}$$

$$- \frac{1}{r\lambda} \frac{\partial f}{\partial r} + \frac{1}{\lambda} \frac{\partial^2 f}{\partial r^2} - \frac{1}{r^2 \lambda} \frac{\partial^2 f}{\partial \theta^2} - \left(\frac{6}{r^3} + \frac{2\sigma}{r\lambda}\right) \frac{\partial u}{\partial r} + \frac{6}{r^3} \frac{\partial^2}{\partial \theta^2} \frac{\partial u}{\partial r} \tag{3.37}$$

2. Example of the construction of the extension operator in case of the elliptical domains, and elliptical angle θ as the parametrization parameter, $\vartheta \equiv \theta$: Analogously to the above case of a circular domain, for the case of the domain where boundary Γ is defined by an ellipse $x^2/a^2 + y^2/b^2 = 1$, one possible convenient choice is to employ elliptical angle θ as the parametrization parameter $\vartheta \equiv \theta$, and represent the extension operators (3.27)–(3.28) using such parametrization (see also [22]).

Recall, that an elliptical coordinate system with coordinates (η, θ) is given by the standard transformation:

$$x = \rho \cosh \eta \cos \theta \tag{3.38}$$

$$y = \rho \sinh \eta \sin \theta \tag{3.39}$$

where $\eta \geq 0$ and $0 \leq \theta < 2\pi$, see Fig. 4. Also, recall that the distance from the center of the ellipse to either foci is defined as $\rho = \sqrt{a^2 - b^2}$.

In elliptical coordinates, the constant $\eta = \eta_0 \equiv \frac{1}{2} \ln \frac{a+b}{a-b}$, the coordinate line (isoline), is given by the ellipse:

$$\frac{x^2}{\rho^2 \cosh^2 \eta_0} + \frac{y^2}{\rho^2 \sinh^2 \eta_0} = 1$$

Similarly, for constant $\theta = \theta_0$, the coordinate line is defined by the hyperbola:

$$\frac{x^2}{\rho^2 \cos^2 \theta_0} - \frac{y^2}{\rho^2 \sin^2 \theta_0} = \cosh^2 \eta - \sinh^2 \eta = 1$$

Now, let us recall that for the choice of elliptical coordinates the basis vectors are defined as:

$$\hat{\eta} = (\rho \sinh \eta \cos \theta, \rho \cosh \eta \sin \theta) \tag{3.40}$$

$$\hat{\theta} = (-\rho \cosh \eta \sin \theta, \rho \sinh \eta \cos \theta) \tag{3.41}$$

The corresponding Lamé coefficients in both directions are equivalent to $H = \rho \sqrt{\sinh^2 \eta + \sin^2 \theta}$. Consequently, the elliptic equation in (3.1) can be rewritten in the standard elliptical coordinates (η, θ) as:

$$\frac{\lambda}{H^2} \left(\frac{\partial^2 u}{\partial \eta^2} + \frac{\partial^2 u}{\partial \theta^2} \right) - \sigma u = f \tag{3.42}$$

Similarly to the above example of a circular domain, the smooth extension operators (3.27)–(3.28) are equivalent to:

$$\pi_{\gamma\Gamma}[\mathbf{u}_\Gamma] \equiv u_{j,k}(\eta_0, \theta) = u \Big|_\Gamma + d \frac{\partial u}{\partial \eta} \Big|_\Gamma + \frac{d^2}{2} \frac{\partial^2 u}{\partial \eta^2} \Big|_\Gamma \tag{3.43}$$

and

$$\pi_{\gamma\Gamma}[\mathbf{u}_\Gamma] \equiv u_{j,k}(\eta_0, \theta) = u \Big|_\Gamma + d \frac{\partial u}{\partial \eta} \Big|_\Gamma + \frac{d^2}{2!} \frac{\partial^2 u}{\partial \eta^2} \Big|_\Gamma + \frac{d^3}{3!} \frac{\partial^3 u}{\partial \eta^3} \Big|_\Gamma + \frac{d^4}{4!} \frac{\partial^4 u}{\partial \eta^4} \Big|_\Gamma \tag{3.44}$$

where, again as before, $d = \eta - \eta_0$ denotes the *signed* distance from a grid point $(x_j, y_k) \in \gamma$ on the coordinate line η , to the nearest point $(x, y) \in \Gamma$ on the original ellipse corresponding to the contour line η_0 .

The higher-order derivatives $\frac{\partial^e u}{\partial \eta^e}$, $e = 2, 3, \dots$ on Γ in (3.43)–(3.44) can be obtained through the Cauchy data $(u(\theta)|_\Gamma, \frac{\partial u}{\partial \eta}(\theta)|_\Gamma)$, and the consecutive differentiation of the governing differential equation (3.42) with respect to η as illustrated below (note that in polar coordinates we had that $\frac{\partial u}{\partial n} = \frac{\partial u}{\partial r}$, but in elliptical coordinates we have $\frac{\partial u}{\partial n} = \frac{1}{H} \frac{\partial u}{\partial \eta}$):

$$\frac{\partial^2 u}{\partial \eta^2} = \frac{H^2}{\lambda} (f + \sigma u) - \frac{\partial^2 u}{\partial \theta^2} \quad (3.45)$$

$$\frac{\partial^3 u}{\partial \eta^3} = 2 \frac{H}{\lambda} \frac{\partial H}{\partial \eta} (f + \sigma u) + \frac{H^2}{\lambda} \left(\frac{\partial f}{\partial \eta} + \sigma \frac{\partial u}{\partial \eta} \right) - \frac{\partial^3 u}{\partial \theta^2 \partial \eta} \quad (3.46)$$

$$\frac{\partial^4 u}{\partial \eta^4} = \frac{2}{\lambda} \left(\left(\frac{\partial H}{\partial \eta} \right)^2 + H \frac{\partial^2 H}{\partial \eta^2} \right) (f + \sigma u) + 4 \frac{H}{\lambda} \frac{\partial H}{\partial \eta} \left(\frac{\partial f}{\partial \eta} + \sigma \frac{\partial u}{\partial \eta} \right) + \frac{H^2}{\lambda} \left(\frac{\partial^2 f}{\partial \eta^2} + \sigma \frac{\partial^2 u}{\partial \eta^2} \right) - \frac{\partial^4 u}{\partial \eta^2 \partial \theta^2} \quad (3.47)$$

where $\frac{\partial^4 u}{\partial \eta^2 \partial \theta^2}$ is given by:

$$\frac{\partial^4 u}{\partial \eta^2 \partial \theta^2} = \frac{2}{\lambda} \left(\left(\frac{\partial H}{\partial \theta} \right)^2 + H \frac{\partial^2 H}{\partial \theta^2} \right) (f + \sigma u) + 4 \frac{H}{\lambda} \frac{\partial H}{\partial \theta} \left(\frac{\partial f}{\partial \theta} + \sigma \frac{\partial u}{\partial \theta} \right) + \frac{H^2}{\lambda} \left(\frac{\partial^2 f}{\partial \theta^2} + \sigma \frac{\partial^2 u}{\partial \theta^2} \right) - \frac{\partial^4 u}{\partial \theta^4} \quad (3.48)$$

Note, that in formulas (3.47)–(3.48) term $\frac{\partial^2 u}{\partial \eta^2}$ is replaced by expression given in (3.45).

After the selection of the parametrization ϑ of Γ and construction of the extension operator, we use spectral approximation (3.30) in the extension operator $u_\gamma = \pi_{\gamma\Gamma}[\tilde{u}_\Gamma]$ in (3.27) (for the second-order method), or in the extension operator $u_\gamma = \pi_{\gamma\Gamma}[\tilde{u}_\Gamma]$ in (3.28) (for the fourth-order method):

$$u_\gamma = \sum_{v=0}^{\mathcal{N}^0} c_v^0 \pi_{\gamma\Gamma}[\Phi_v^0(\vartheta)] + \sum_{v=0}^{\mathcal{N}^1} c_v^1 \pi_{\gamma\Gamma}[\Phi_v^1(\vartheta)]. \quad (3.49)$$

Therefore, boundary equations (BEP) (3.26) becomes an overdetermined linear system of the dimension $|\gamma| \times (\mathcal{N}^0 + \mathcal{N}^1)$ for the unknowns (c_v^0, c_v^1) (note that in general we can assume $|\gamma| \gg (\mathcal{N}^0 + \mathcal{N}^1)$). This system (3.26) for (c_v^0, c_v^1) is solved using the least-squares method, and hence one obtains the unknown density u_γ .

The final step of the DPM is to use the computed density u_γ to construct the approximation to the solution (3.1)–(3.2) inside the physical domain Ω .

Generalized Green's Formula:

Statement 3.5. The discrete solution $u_{j,k} := \mathbf{P}_{N+\gamma} u_\gamma + G^h f$, $(x_j, y_k) \in N^+$ is the approximation to the exact solution $u(x_j, y_k)$, $(x_j, y_k) \in N^+ \cap \Omega$ of the continuous problem (3.1)–(3.2).

Discussion. The result is the consequence of the sufficient regularity of the exact solution, Theorem 3.4, either the extension operator (3.27) (for the second-order scheme) or the extension operator (3.28) (for the fourth-order scheme), as well as the second-order and the fourth-order accuracy of the schemes (3.16), (3.17) respectively. Thus, we expect that the numerical solution $u_{j,k} := \mathbf{P}_{N+\gamma} u_\gamma + G^h f$ will approximate the exact solution $u(x_j, y_k)$, $(x_j, y_k) \in N^+ \cap \bar{\Omega}$ of the continuous problem (3.1)–(3.2) with $O(h^2)$ (for the second-order scheme) and with $O(h^4)$ (for the fourth-order scheme) in the maximum norm. Furthermore, in Section 6, we confirm the efficiency and the high-order accuracy of the proposed numerical algorithms with several challenging numerical tests for the interface/composite domain problems.

Recall, in [28,29] it was shown (under sufficient regularity of the exact solution), that the Difference Potentials approximate surface potentials of the elliptic operators (and, therefore DPM approximates the solution to the elliptic boundary value problem) with the accuracy of $O(h^{\mathcal{P}-\varepsilon})$ in the discrete Hölder norm of order $\mathcal{Q} + \varepsilon$. Here, $0 < \varepsilon < 1$ is an arbitrary number, \mathcal{Q} is the order of the considered elliptic operator, and \mathcal{P} is the order of the numerical scheme used for the approximation of the elliptic operator, see [28,29] or [31] for the details and proof of the general result. \square

Remark.

- The formula $\mathbf{P}_{N+\gamma} u_\gamma + G^h f$ is the *discrete generalized Green's formula*.
- Note that after the density u_γ is reconstructed from the *Boundary Equations with Projection* (3.26), the Difference Potential is easily obtained as the solution of a simple (AP) using Definition 3.3.

4. Schemes based on difference potentials for interface and composite domains problems

In Section 3.2 we constructed second and fourth-order schemes based on Difference Potentials for problems in the single domain Ω . In this section, we will show how to extend these methods to interface/composite domains problems (2.1)–(2.3).

First, as we have done in Section 3 for the single domain Ω , we will introduce the auxiliary domains. We will place each of the original subdomains Ω_s in the auxiliary domains $\Omega_s^0 \subset \mathbb{R}^2$, ($s = 1, 2$) and will state the auxiliary difference problems in each subdomain Ω_s , ($s = 1, 2$). The choice of these auxiliary domains Ω_1^0 and Ω_2^0 , as well as the auxiliary difference problems, do not need to depend on each other. After that, for each subdomain, we will proceed in a similar way as we did in Section 3.2. Also, for each auxiliary domain Ω_s^0 we will consider, for example a Cartesian mesh (the choice of the grids for the auxiliary problems will be independent of each other). After that, all the definitions, notations, and properties introduced in Section 3.2 extend to each subdomain Ω_s in a direct way (index s , ($s = 1, 2$) is used to distinguish each subdomain). Let us denote the difference problem of (2.1)–(2.3) for each subdomain as:

$$L_h^s[u_{j,k}] = f_{s,j,k}, \quad (x_j, y_k) \in M_s^+ \tag{4.1}$$

The difference problem (4.1) is obtained using either the second-order (3.16) or the fourth-order scheme (3.17).

The main theorem of the method for the composite domains/interface problems is:

Statement 4.1. Density $u_\gamma := (u_{\gamma_1}, u_{\gamma_2})$ is the trace of some solution u , $(x_j, y_k) \in \Omega_1 \cup \Omega_2$ to the Difference Equations (4.1): $u_\gamma \equiv Tr_\gamma u$, if and only if, the following equalities hold

$$u_{\gamma_1} = \mathbf{P}_{\gamma_1} u_{\gamma_1} + G^h f_{\gamma_1}, \quad (x_j, y_k) \in \gamma_1 \tag{4.2}$$

$$u_{\gamma_2} = \mathbf{P}_{\gamma_2} u_{\gamma_2} + G^h f_{\gamma_2}, \quad (x_j, y_k) \in \gamma_2 \tag{4.3}$$

The obtained discrete solution $u_{j,k} := \mathbf{P}_{N_s^+ \gamma_s} u_{\gamma_s} + G_s^h f_s$, $(x_j, y_k) \in N_s^+$ is the approximation to the exact solution $u(x_j, y_k)$, $(x_j, y_k) \in N_s^+ \cap \Omega_s$ of the continuous model problem (2.1)–(2.3). Here, index $s = 1, 2$.

Discussion. The result is a consequence of the results in Section 3.2. We expect that the solution $u_{j,k} := \mathbf{P}_{N_s^+ \gamma_s} u_{\gamma_s} + G_s^h f_s$, $(x_j, y_k) \in N_s^+$ will approximate the exact solution $u(x_j, y_k)$, $(x_j, y_k) \in N_s^+ \cap \tilde{\Omega}_s$, ($s = 1, 2$) with the accuracy $O(h^2)$ for the second-order method, and with the accuracy $O(h^4)$ for the fourth-order method in the maximum norm. Also, see Section 6 for the numerical results. \square

Remark. Similar to the discussion in Section 3.2, the Boundary Equations (4.2)–(4.3) alone will have multiple solutions and have to be coupled with boundary (2.3) and interface conditions (2.2) to obtain the unique densities u_{γ_1} and u_{γ_2} . We consider the extension formula (3.27) (second-order method) or (3.28) (fourth-order method) to construct u_{γ_s} , $s = 1, 2$ in each subdomain/domain.

5. Main steps of the algorithm

In this section, for the reader's convenience we will briefly summarize the main steps of the numerical algorithm.

- Step 1: Introduce a computationally simple auxiliary domain and formulate the auxiliary problem (AP).
- Step 2: Compute a Particular solution, $u_{j,k} := G^h f$, $(x_j, y_k) \in N^+$, as the solution of the (AP). For the single domain method, see (3.20)–(3.21) in Section 3.2 (second-order and fourth-order schemes). For the direct extension of the algorithms to the interface and composite domains problems, see Section 4.
- Step 3: Next, compute the unknown densities u_γ at the points of the discrete grid boundary γ by solving the system of linear equations derived from the system of Boundary Equations with Projection: see (3.26)–(3.27) (second-order scheme), or (3.26), (3.28) (fourth-order scheme) in Section 3.2, and extension to the interface and composite domain problems (4.2)–(4.3) in Section 4.
- Step 4: Using the definition of the Difference Potential, Definition 3.3, Section 3.2, and Section 4 (algorithm for interface/composite domain problems), compute the Difference Potential $\mathbf{P}_{N^+ \gamma} u_\gamma$ from the obtained density u_γ .
- Step 5: Finally, obtain the approximation to the continuous solution from u_γ using the generalized Green's formula, $u(x, y) \approx \mathbf{P}_{N^+ \gamma} u_\gamma + G^h f$, see Statement 3.5 in Section 3.2, and see Statement 4.1 in Section 4.

6. Numerical tests

In this section, we present several numerical experiments for interface/composite domain problems that illustrate the high-order accuracy and efficiency of methods based on Difference Potentials presented in Sections 2–4. Moreover, we also compare the accuracy of Difference Potentials methods with the accuracy of some established methods for interface

problems, like Mayo's method [21,4], and Immersed Interface method (IIM) [15,4], as well as with the accuracy of a recently developed Finite Element method, Edge-Based Correction Finite Element Interface method (EBC-FEI), [13].

In all the numerical tests below, except the first test from [13] Table 1, the error in the approximation E to the exact solution of the model is determined by the size of the *relative* maximum error:

$$E := \frac{\max_{(x_j, y_k) \in M_1^+ \cup M_2^+} |u(x_j, y_k) - u_{j,k}|}{\max_{(x_j, y_k) \in M_1^+ \cup M_2^+} |u(x_j, y_k)|} \quad (6.1)$$

Moreover, we also compute the *relative* maximum error in the components of the discrete gradient denoted E_{∇_x} and E_{∇_y} , which are determined by the following centered difference formulas:

$$E_{\nabla_x} := \frac{\max_{(x_i, y_j) \in M_1^+ \cup M_2^+} \left| \frac{u(x_j+h, y_k) - u(x_j-h, y_k)}{2h} - \frac{u_{j+1,k} - u_{j-1,k}}{2h} \right|}{\max_{(x_j, y_k) \in M_1^+ \cup M_2^+} \left| \frac{u(x_j+h, y_k) - u(x_j-h, y_k)}{2h} \right|} \quad (6.2)$$

$$E_{\nabla_y} := \frac{\max_{(x_i, y_j) \in M_1^+ \cup M_2^+} \left| \frac{u(x_j, y_k+h) - u(x_j, y_k-h)}{2h} - \frac{u_{j,k+1} - u_{j,k-1}}{2h} \right|}{\max_{(x_j, y_k) \in M_1^+ \cup M_2^+} \left| \frac{u(x_j, y_k+h) - u(x_j, y_k-h)}{2h} \right|} \quad (6.3)$$

In the first test below from [13], Section 6.1, Table 1, we compute just maximum error in the solution E^m and in the discrete gradient of the solution $E_{\nabla_x}^m$ and $E_{\nabla_y}^m$.

Remarks.

- Below, in Sections 6.1–6.4 we consider interface/composite domain problems defined in domains similar to the example of the domains Ω_1 and Ω_2 illustrated on Fig. 1, Section 1. Hence, for the exterior domain Ω_1 we select auxiliary domain Ω_1^0 to be a rectangle with the boundary $\partial\Omega_1^0$, which coincides with the exterior boundary $\partial\Omega_1$ of the exterior domain Ω_1 . After that, we construct our method based on Difference Potentials as described in Sections 3.2–5. To take advantage of the given boundary conditions and specifics of the exterior domain Ω_1 /auxiliary domain Ω_1^0 , we construct the particular solution (3.20) and Difference Potential (3.22) for the exterior auxiliary problem in Ω_1^0 using the discrete operator $L_h[u_{j,k}]$. This discrete operator has a modified stencil near the boundary of the auxiliary domain Ω_1^0 for the fourth-order method (3.17) as follows (example of the point at “southwest” corner of the grid):

$$\begin{aligned} L_h^1[u_{1,1}] = & \lambda_1 \frac{10u_{0,1} - 15u_{1,1} - 4u_{2,1} + 14u_{3,1} - 6u_{4,1} + u_{5,1}}{12h^2} \\ & + \lambda_1 \frac{10u_{1,0} - 15u_{1,1} - 4u_{1,2} + 14u_{1,3} - 6u_{1,4} + u_{1,5}}{12h^2} - \sigma_1 u_{1,1}, \text{ in } \Omega_1^0. \end{aligned} \quad (6.4)$$

Other near-boundary nodes in Ω_1^0 are handled in a similar way in $L_h[u_{j,k}]$ for (3.17) (fourth-order scheme).

Note, that to construct a particular solution (3.20) and Difference Potential (3.22) for the interior problem stated in auxiliary domain Ω_2^0 , we do not modify stencil in $L_h[u_{j,k}]$ for (3.17) (fourth-order scheme) near the boundary $\partial\Omega_2^0$ of the interior auxiliary domain Ω_2^0 .

- In all numerical tests in Sections 6.1–6.4, we select a standard trigonometric system of basis functions for the spectral approximation in (3.30), Section 3.2: $\phi_0(\vartheta) = 1, \phi_1(\vartheta) = \sin\left(\frac{2\pi}{|\Gamma|}\vartheta\right), \phi_2(\vartheta) = \cos\left(\frac{2\pi}{|\Gamma|}\vartheta\right), \dots, \phi_{2\nu}(\vartheta) = \cos\left(\frac{2\pi\nu}{|\Gamma|}\vartheta\right)$ and $\phi_{2\nu+1}(\vartheta) = \sin\left(\frac{2\pi\nu}{|\Gamma|}\vartheta\right), \nu = 0, 1, 2, \dots$. Here, $\phi_\nu \equiv \phi_\nu^0 \equiv \phi_\nu^1$.

6.1. Second-order (DPM2) and fourth-order (DPM4): comparison with EBC-FEI, IIM and Mayo's methods

The first test that we consider below (6.5)–(6.6) can be found in a recent paper, on Edge-Based Correction Finite Element Interface method (EBC-FEI), [13], and a similar test problem was considered also in [15]. In this test we illustrate that DPM2 and DPM4 capture the solution and the discrete gradient of the solution with almost machine-accuracy (compare to EBC-FEI results in [13]). The test problem is defined similar to [13]:

$$\Delta u = 0, \quad (6.5)$$

subject to the interface and boundary conditions in the form of (2.2)–(2.3) (computed using the exact solution and Dirichlet boundary condition on the boundary of the exterior domain $\partial\Omega_1$). The exact solution for the test problem is

$$u(x, y) = \begin{cases} u_1(x, y) = 0, & (x, y) \in \Omega_1, \\ u_2(x, y) = x^2 - y^2, & (x, y) \in \Omega_2. \end{cases} \quad (6.6)$$

Table 1

Grid convergence in the approximate solution and components of the discrete gradient for DPM2 (left) and DPM4 (right). Here, we selected N to match h in the paper, [13]: $N = 45$ corresponds to $h \approx 4.4e-02$ and $N = 1438$ corresponds to $h = 1.4e-03$. The interior domain Ω_2 is the circle with $R = \frac{2}{3}$ centered at the origin, and the exterior domain is $\Omega_1 = [-1, 1] \times [-1, 1] \setminus \Omega_2$. The dimension of the set of basis functions is $\mathcal{N}^0 + \mathcal{N}^1 = 2$.

N	E^m : DPM2	E^m : DPM4
45	4.9960E-16	6.1062E-16
89	1.2930E-15	5.2180E-15
179	2.7756E-16	1.3656E-14
360	1.6653E-15	1.7855E-15
719	1.8282E-15	1.9335E-13
1438	1.1191E-15	7.8770E-13
N	$E_{\nabla_x}^m$: DPM2	$E_{\nabla_x}^m$: DPM4
45	4.3299E-15	6.2728E-15
89	1.0436E-14	2.2204E-14
179	1.9873E-14	6.7057E-14
360	5.7399E-14	7.5051E-14
719	1.2468E-13	8.8818E-13
1438	2.8433E-13	3.5123E-12
N	$E_{\nabla_y}^m$: DPM2	$E_{\nabla_y}^m$: DPM4
45	3.1086E-15	3.7470E-15
89	8.6597E-15	2.4647E-14
179	1.2434E-14	7.1942E-14
360	4.4964E-14	5.9952E-14
719	1.0991E-13	8.8818E-13
1438	2.5935E-13	3.4326E-12

The interior subdomain and exterior subdomain for the test problem are:

$$\Omega_2 = x^2 + y^2 < \frac{4}{9}, \text{ interior subdomain,}$$

$$\Omega_1 = [-1, 1] \times [-1, 1] \setminus \Omega_2, \text{ exterior subdomain.}$$

We employ for DPM the following auxiliary domains here:

$$\Omega_1^0 \equiv \Omega_2^0 = [-1, 1] \times [-1, 1].$$

Table 1 (maximum error in the solution and the maximum error in the components of discrete gradient of the solution) clearly illustrate almost machine precision accuracy for DPM2 and DPM4 as expected on such a test problem (the observed slight breakdown of the accuracy of the fourth-order scheme DPM4 on finer grids is due to the loss of significant digits).

The other tests presented in Tables 2–26, Sections 6.1–6.3 consider ellipses $\frac{x^2}{a^2} + \frac{y^2}{b^2} = 1$ with a different aspect ratio a/b as the interface curve. Note that we also performed the same tests using a circle as the interface curve and obtained a similar convergence rate: second-order and fourth-order convergence rate in the maximum error in the solution, as well as in the maximum error in the discrete gradient of the solution for DPM2 and DPM4, respectively. Furthermore, results presented in Fig. 5 show that the error in the solution in DPM (DPM2 and DPM4) is not affected too much by the size of the aspect ratio of the considered elliptical domains. This demonstrates the additional robustness of the designed numerical schemes.

The test problems for Tables 2–3 are defined similar to [4]:

$$\Delta u_s = f_s, \quad s = 1, 2 \tag{6.7}$$

subject to the interface and boundary conditions in the form of (2.2)–(2.3) (computed using the exact solutions and Dirichlet boundary condition on the boundary of the exterior domain $\partial\Omega_1$). The exact solution, see Fig. 6, for the test problem in [4], page 110 and in Table 2 is defined as

$$u(x, y) = \begin{cases} u_1(x, y) = 0, & (x, y) \in \Omega_1, \\ u_2(x, y) = \sin x \cos y, & (x, y) \in \Omega_2 \end{cases} \tag{6.8}$$

The exact solution, see Fig. 6 for the test problem in [4], page 112 and in Table 3 is defined as

$$u(x, y) = \begin{cases} u_1(x, y) = 0, & (x, y) \in \Omega_1, \\ u_2(x, y) = x^9 y^8, & (x, y) \in \Omega_2. \end{cases} \tag{6.9}$$

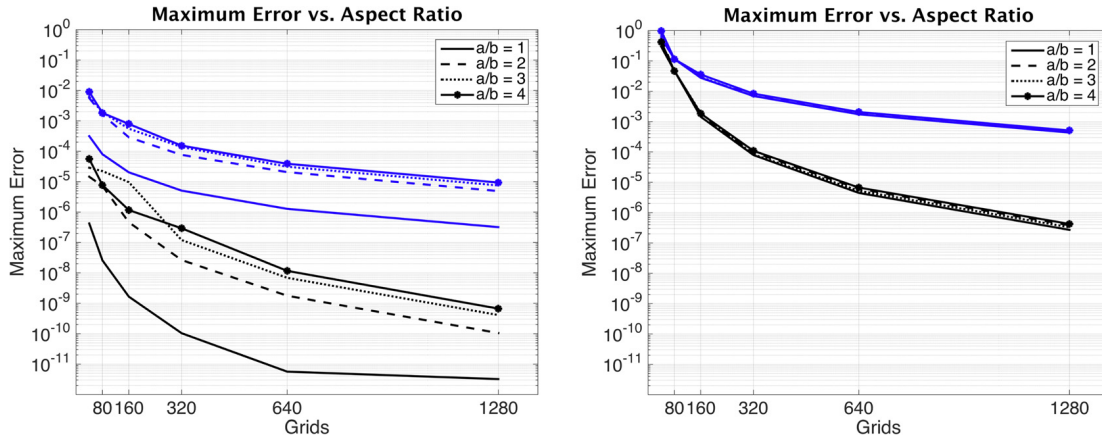


Fig. 5. Grid convergence using DPM2 (blue) and DPM4 (black) is compared for several different interfaces $\Gamma : x^2/a^2 + y^2/b^2 = 1$ with increasing aspect ratios a/b . The results are presented for the test problem (6.10), (6.11) with material coefficients $\lambda_1 = \lambda_2 = 1$ (left figure) and for the test problem (6.10), (6.12) with material coefficients $\lambda_1 = \lambda_2 = 1$ (right figure). Similar results are produced by DPM for the same test problems but with different material coefficients in different subdomains, as well as for error in the gradient of the solution. (For interpretation of the references to color in this figure legend, the reader is referred to the web version of this article.)

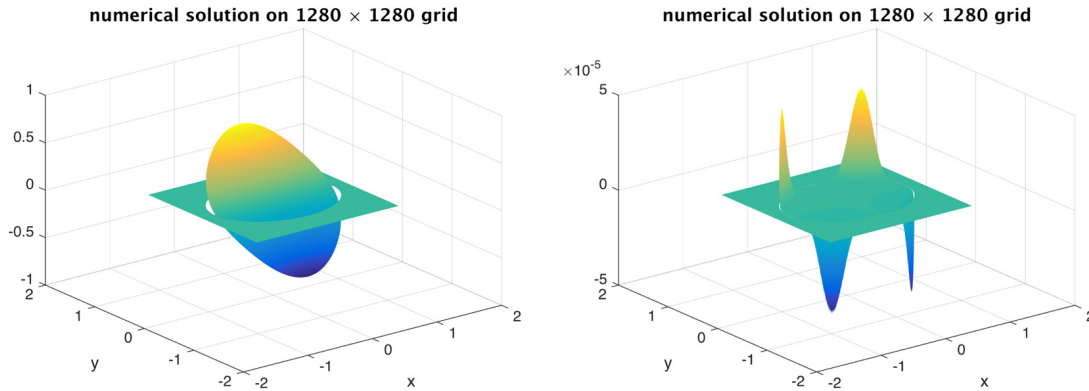


Fig. 6. Plot of the numerical solution corresponding to (6.8) using DPM4 (left). Plot of the numerical solution corresponding to (6.9) using DPM4 (right).

The interior domain and exterior domains for both test problems are:

$$\Omega_2 = \frac{x^2}{0.49} + \frac{y^2}{0.81} < 1,$$

$$\Omega_1 = [-1.1, 1.1] \times [-1.1, 1.1] \setminus \Omega_2.$$

Again, to use similar (but not exact) settings as in [4] we employ for DPM2 and DPM4 the following auxiliary domains here:

$$\Omega_1^0 = [-1.1, 1.1] \times [-1.1, 1.1],$$

$$\Omega_2^0 = [-1.375, 1.375] \times [-1.375, 1.375].$$

Results in Tables 2–3 for DPM2 illustrate overall second-order rate of convergence in the relative maximum error in the solution and in the relative maximum error in the discrete gradient of the solution, and are either similar or better than the results for Mayo’s method and IIM for the same test problems in [4]. Moreover, DPM4 gives a fourth-order convergence rate in the relative maximum error in the solution and in the relative maximum error in the discrete gradient of the solution, and the magnitude of the errors is much smaller than for DPM2, Mayo’s method and IIM. *Such high-order accuracy of DPM4 and the efficiency of numerical algorithms based on Difference Potentials is also crucial for time-dependent problems where lower-order methods will fail to resolve delicate features of the solutions to model problems [1,2].* Note, that we also used here different auxiliary domains for the interior and exterior subdomains – this is another flexibility of DPM. Let us mention that the observed breakdown of the accuracy of the DPM4 on the finer grid in Table 2 is due to the loss of significant digits, as the absolute levels of error get closer to machine zero. Finally, let us comment that for the elliptic models, DPM2 can be more computationally expensive (but more accurate) than the second-order Mayo’s method or the second-order IIM. The overall computational complexity of the proposed algorithms based on Difference Potentials is the repeated solution of the simple discrete AP (3.18)–(3.19) (it needs to be solved about $\mathcal{N}_1 + \mathcal{N}_2$ times). But, only the right-hand side of the AP changes

Table 2

Grid convergence in the approximate solution and components of the discrete gradient for DPM2 (left) and DPM4 (right). The interior domain Ω_2 is the ellipse with $a = 0.7$, $b = 0.9$ centered at the origin, and the exterior domain is $[-1.1, 1.1] \times [-1.1, 1.1] \setminus \Omega_2$. Test problem (6.7)–(6.8). The dimension of the set of basis functions is $\mathcal{N}^0 + \mathcal{N}^1 = 2$. In this test N denotes half of the number of subintervals in each direction as in [4]; compare results to [4] Table 1 (top), page 111.

N	E: DPM2	Rate	E: DPM4	Rate
40	2.4180E–05	–	1.7270E–08	–
80	3.4680E–06	2.80	6.6025E–10	4.71
160	8.8833E–07	1.96	4.4058E–11	3.91
320	1.6222E–07	2.45	2.0658E–12	4.41
640	2.5862E–08	2.65	1.5394E–13	3.75
N	E_{∇_x} : DPM2	Rate	E_{∇_x} : DPM4	Rate
40	1.7073E–04	–	1.1793E–07	–
80	4.6437E–05	1.88	9.1058E–09	3.70
160	1.1223E–05	2.05	5.8895E–10	3.95
320	3.0797E–06	1.87	3.7220E–11	3.98
640	8.2122E–07	1.91	1.9138E–11	0.96
N	E_{∇_y} : DPM2	Rate	E_{∇_y} : DPM4	Rate
40	1.2071E–04	–	8.8412E–08	–
80	3.3660E–05	1.84	6.1055E–09	3.86
160	8.4065E–06	2.00	3.8586E–10	3.98
320	2.0770E–06	2.02	2.5030E–11	3.95
640	5.2512E–07	1.98	1.6489E–11	0.60

Table 3

Grid convergence in the approximate solution and components of the discrete gradient for DPM2 (left) and DPM4 (right). The interior domain Ω_2 is the ellipse with $a = 0.7$, $b = 0.9$ centered at the origin, and the exterior domain is $[-1.1, 1.1] \times [-1.1, 1.1] \setminus \Omega_2$. Test problem (6.7), (6.9). The dimension of the set of basis functions is $\mathcal{N}^0 + \mathcal{N}^1 = 2$. In this test N denotes half of the number of subintervals in each direction as in [4]; compare results to [4] Table 2, page 112.

N	E: DPM2	Rate	E: DPM4	Rate
40	2.0806E–04	–	9.8715E–05	–
80	1.6632E–04	0.32	3.0595E–06	5.01
160	2.6204E–05	2.67	2.0603E–07	3.89
320	2.7635E–06	3.25	9.0652E–09	4.51
640	8.5375E–07	1.69	3.5813E–10	4.66
N	E_{∇_x} : DPM2	Rate	E_{∇_x} : DPM4	Rate
40	1.3244E–02	–	3.1656E–04	–
80	3.6334E–03	1.87	1.7578E–05	4.17
160	8.0133E–04	2.18	1.0516E–06	4.06
320	2.1239E–04	1.92	6.4620E–08	4.02
640	5.8496E–05	1.86	4.0180E–09	4.01
N	E_{∇_y} : DPM2	Rate	E_{∇_y} : DPM4	Rate
40	1.8164E–02	–	3.9253E–04	–
80	3.9592E–03	2.20	2.1308E–05	4.20
160	1.1045E–03	1.84	1.2480E–06	4.09
320	2.8151E–04	1.97	7.5577E–08	4.05
640	6.6274E–05	2.09	4.6188E–09	4.03

and $\mathcal{N}_1 + \mathcal{N}_2 \ll |\gamma_s|$, thus the repeated solutions of the AP (3.18)–(3.19) can be done very efficiently. Here, $|\gamma_s|$, ($s = 1, 2$) is the cardinality of the discrete boundary set.

6.2. Second-order (DPM2) and fourth-order (DPM4): additional numerical tests

The next several tests are modified versions of the test problem from [17]. Furthermore, we consider an interface model problem (2.1) with different diffusion/material coefficients in different subdomains (including a large jump ratio between diffusion/material coefficients λ_1 in Ω_1 and λ_2 in Ω_2) which makes it an even more challenging task for numerical methods. In all the following tables, N denotes the total number of subintervals in each direction. The test problems for Tables 4–12 are defined similar to [17]:

$$\nabla \cdot (\lambda_s \nabla u_s) = f_s, \quad s = 1, 2 \tag{6.10}$$

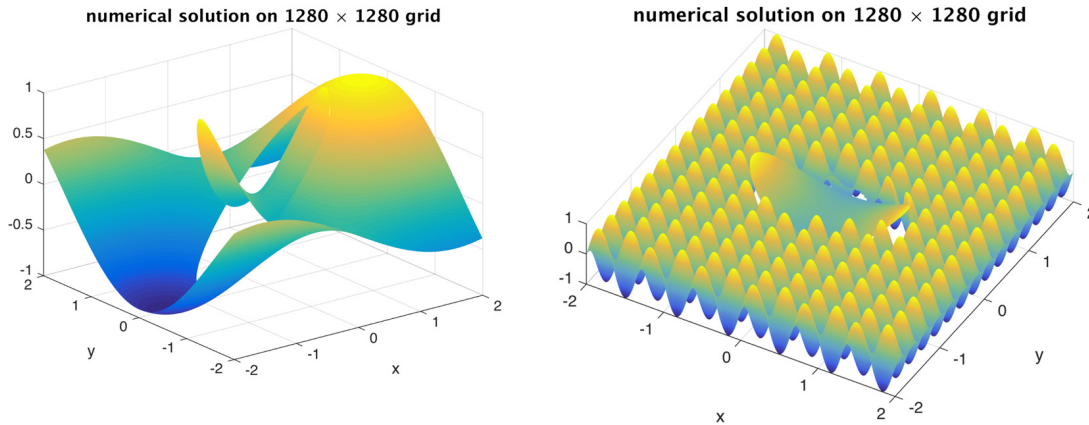


Fig. 7. Plot of the numerical solution using DPM4 corresponding to (6.11) with interface defined by the ellipse $\Gamma : x^2 + 4y^2 = 1$ (left figure). Plot of the numerical solution using DPM4 corresponding to (6.12) with interface defined by the ellipse $\Gamma : x^2 + 4y^2 = 1$ (right figure).

Table 4

Grid convergence in the approximate solution and components of the discrete gradient for DPM2 (left) and DPM4 (right). The interior domain Ω_2 is the ellipse with $a = 1, b = 0.5$ centered at the origin, and the exterior domain is $\Omega_1 = [-2, 2] \times [-2, 2] \setminus \Omega_2$. Test problem (6.10), (6.11) with material coefficients $\lambda_1 = \lambda_2 = 1$. The dimension of the set of basis functions is $\mathcal{N}^0 + \mathcal{N}^1 = 17$.

N	E: DPM2	Rate	E: DPM4	Rate
160	2.8834E-04	–	4.6351E-07	–
320	7.6116E-05	1.92	2.6459E-08	4.13
640	2.0678E-05	1.88	1.7726E-09	3.90
1280	4.9212E-06	2.07	1.0498E-10	4.08
N	E_{∇_x} : DPM2	Rate	E_{∇_x} : DPM4	Rate
160	5.5817E-04	–	6.7908E-07	–
320	1.5141E-04	1.88	4.4384E-08	3.94
640	4.5776E-05	1.73	2.8536E-09	3.96
1280	1.1892E-05	1.94	1.8609E-10	3.94
N	E_{∇_y} : DPM2	Rate	E_{∇_y} : DPM4	Rate
160	5.5629E-04	–	9.3938E-07	–
320	1.3835E-04	2.01	3.9553E-08	4.57
640	3.5578E-05	1.96	2.7175E-09	3.86
1280	9.3981E-06	1.92	1.7772E-10	3.93

subject to the interface and boundary conditions in the form of (2.2)–(2.3) (computed using the exact solutions and Dirichlet boundary condition on the boundary of the exterior domain $\partial\Omega_1$). The exact solution for the test problem in Tables 4–12, see also Fig. 7 (and in [17]) is defined as

$$u(x, y) = \begin{cases} u_1(x, y) = \sin x \cos y, & (x, y) \in \Omega_1, \\ u_2(x, y) = x^2 - y^2, & (x, y) \in \Omega_2. \end{cases} \tag{6.11}$$

Moreover, the exact solution for the test problem in Tables 13–26 has a much higher frequency (oscillations) in the exterior subdomain Ω_1 , see Fig. 7, and is defined as:

$$u(x, y) = \begin{cases} u_1(x, y) = \sin 3\pi x \cos 7\pi y, & (x, y) \in \Omega_1, \\ u_2(x, y) = x^2 - y^2, & (x, y) \in \Omega_2. \end{cases} \tag{6.12}$$

The interior domain and exterior domains for both test problems are:

$$\Omega_2 = \frac{x^2}{a^2} + \frac{y^2}{b^2} < 1,$$

$$\Omega_1 = [-2, 2] \times [-2, 2] \setminus \Omega_2.$$

We employ for DPM the following auxiliary domains here:

$$\Omega_1^0 \equiv \Omega_2^0 = [-2, 2] \times [-2, 2].$$

As in previous tests, results in Tables 4–21 illustrate an overall second-order rate of convergence for DPM2, and fourth-order convergence rate for DPM4 in the relative maximum error in the solution and in the relative maximum error in

Table 5

Grid convergence in the approximate solution and components of the discrete gradient for DPM2 (left) and DPM4 (right). The interior domain Ω_2 is the ellipse with $a = 0.9$, $b = 0.3$ centered at the origin, and the exterior domain is $\Omega_1 = [-2, 2] \times [-2, 2] \setminus \Omega_2$. Test problem (6.10), (6.11) with material coefficients $\lambda_1 = \lambda_2 = 1$. The dimension of the set of basis functions is $\mathcal{N}^0 + \mathcal{N}^1 = 17$.

N	E: DPM2	Rate	E: DPM4	Rate
160	5.5513E-04	–	9.6244E-06	–
320	1.3776E-04	2.01	1.2031E-07	6.32
640	3.1185E-05	2.14	6.8993E-09	4.12
1280	7.5539E-06	2.05	4.1147E-10	4.07
N	E_{∇_x} : DPM2	Rate	E_{∇_x} : DPM4	Rate
160	1.2706E-03	–	2.8293E-05	–
320	3.9571E-04	1.68	2.4007E-07	6.88
640	1.1077E-04	1.84	1.8805E-08	3.67
1280	2.9727E-05	1.90	1.3125E-09	3.84
N	E_{∇_y} : DPM2	Rate	E_{∇_y} : DPM4	Rate
160	1.1064E-03	–	4.1055E-05	–
320	2.5858E-04	2.10	3.1522E-07	7.03
640	7.5354E-05	1.78	1.6035E-08	4.30
1280	2.0664E-05	1.87	1.0850E-09	3.89

Table 6

Grid convergence in the approximate solution and components of the discrete gradient for DPM2 (left) and DPM4 (right). The interior domain Ω_2 is the ellipse with $a = 1$, $b = 0.25$ centered at the origin, and the exterior domain is $\Omega_1 = [-2, 2] \times [-2, 2] \setminus \Omega_2$. Test problem (6.10), (6.11) with material coefficients $\lambda_1 = \lambda_2 = 1$. The dimension of the set of basis functions is $\mathcal{N}^0 + \mathcal{N}^1 = 17$.

N	E: DPM2	Rate	E: DPM4	Rate
160	7.9331E-04	–	1.1962E-06	–
320	1.5312E-04	2.37	2.9307E-07	2.03
640	3.8833E-05	1.98	1.1668E-08	4.65
1280	9.3874E-06	2.05	6.6905E-10	4.12
N	E_{∇_x} : DPM2	Rate	E_{∇_x} : DPM4	Rate
160	1.8881E-03	–	3.9764E-06	–
320	4.5911E-04	2.04	1.0648E-06	1.90
640	1.4552E-04	1.66	3.5132E-08	4.92
1280	4.0391E-05	1.85	2.5001E-09	3.81
N	E_{∇_y} : DPM2	Rate	E_{∇_y} : DPM4	Rate
160	2.1015E-03	–	6.3942E-06	–
320	4.5735E-04	2.20	1.6593E-06	1.95
640	1.1380E-04	2.01	4.3716E-08	5.25
1280	3.1276E-05	1.86	2.2722E-09	4.27

the discrete gradient of the solution. This confirms that designed methods based on Difference Potentials are high-order accurate sharp interface methods, which can also handle irregular geometry efficiently using simple grids.

6.3. Second-order (DPM2) and fourth-order (DPM4): non-matching grids and mixed-order

Finally, we use the same test problem (6.10), (6.12) to illustrate another flexibility of these methods: we consider non-matching grids for different subdomains, see Table 22. We show that when we use a much coarser mesh in the domain Ω_2 with the less oscillatory solution, we obtain an accuracy which is very close to the accuracy we achieved while using the same fine mesh in both domains Ω_1 and Ω_2 , see Table 23. We plan to develop this feature further and design adaptive algorithms based on DPM that will handle geometric singularities. Moreover, for the same test problem, (6.10), (6.12) we consider mixed-order DPM (we use different order of approximation in different domains), Tables 24–25. We also show that when we use a lower order approximation in the domain Ω_2 with a less oscillatory solution, we obtain an accuracy which is very close to the accuracy achieved while using the same high-order approximation in both domains Ω_1 and Ω_2 (and better accuracy when we used the same lower-order in both domains Ω_1 and Ω_2 , see Table 26).

The interior domain and exterior domains in tests in Tables 22–26 are:

$$\Omega_2 = x^2 + 4y^2 < 1,$$

$$\Omega_1 = [-2, 2] \times [-2, 2] \setminus \Omega_2.$$

Table 7

Grid convergence in the approximate solution and components of the discrete gradient for DPM2 (left) and DPM4 (right). The interior domain Ω_2 is the ellipse with $a = 1$, $b = 0.5$ centered at the origin, and the exterior domain is $\Omega_1 = [-2, 2] \times [-2, 2] \setminus \Omega_2$. Test problem (6.10), (6.11) with material coefficients $\lambda_1 = 1000$ and $\lambda_2 = 1$. The dimension of the set of basis functions is $\mathcal{N}^0 + \mathcal{N}^1 = 17$.

N	E: DPM2	Rate	E: DPM4	Rate
160	2.8834E-04	–	4.6351E-07	–
320	7.6116E-05	1.92	2.6459E-08	4.13
640	2.0678E-05	1.88	1.7726E-09	3.90
1280	4.9212E-06	2.07	1.0487E-10	4.08
N	E_{∇_x} : DPM2	Rate	E_{∇_x} : DPM4	Rate
160	5.5817E-04	–	6.7908E-07	–
320	1.5141E-04	1.88	4.4384E-08	3.94
640	4.5776E-05	1.73	2.8536E-09	3.96
1280	1.1892E-05	1.94	1.8604E-10	3.94
N	E_{∇_y} : DPM2	Rate	E_{∇_y} : DPM4	Rate
160	5.5629E-04	–	9.3938E-07	–
320	1.3835E-04	2.01	3.9553E-08	4.57
640	3.5578E-05	1.96	2.7175E-09	3.86
1280	9.3981E-06	1.92	1.7780E-10	3.93

Table 8

Grid convergence in the approximate solution and components of the discrete gradient for DPM2 (left) and DPM4 (right). The interior domain Ω_2 is the ellipse with $a = 0.9$, $b = 0.3$ centered at the origin, and the exterior domain is $\Omega_1 = [-2, 2] \times [-2, 2] \setminus \Omega_2$. Test problem (6.10), (6.11) with material coefficients $\lambda_1 = 1000$ and $\lambda_2 = 1$. The dimension of the set of basis functions is $\mathcal{N}^0 + \mathcal{N}^1 = 17$.

N	E: DPM2	Rate	E: DPM4	Rate
160	5.5513E-04	–	9.6244E-06	–
320	1.3776E-04	2.01	1.2031E-07	6.32
640	3.1185E-05	2.14	6.8993E-09	4.12
1280	7.5539E-06	2.05	4.1143E-10	4.07
N	E_{∇_x} : DPM2	Rate	E_{∇_x} : DPM4	Rate
160	1.2706E-03	–	2.8293E-05	–
320	3.9571E-04	1.68	2.4007E-07	6.88
640	1.1077E-04	1.84	1.8805E-08	3.67
1280	2.9727E-05	1.90	1.3124E-09	3.84
N	E_{∇_y} : DPM2	Rate	E_{∇_y} : DPM4	Rate
160	1.1064E-03	–	4.1055E-05	–
320	2.5858E-04	2.10	3.1522E-07	7.03
640	7.5354E-05	1.78	1.6035E-08	4.30
1280	2.0664E-05	1.87	1.0851E-09	3.89

Table 9

Grid convergence in the approximate solution and components of the discrete gradient for DPM2 (left) and DPM4 (right). The interior domain Ω_2 is the ellipse with $a = 1$, $b = 0.25$ centered at the origin, and the exterior domain is $\Omega_1 = [-2, 2] \times [-2, 2] \setminus \Omega_2$. Test problem (6.10), (6.11) with material coefficients $\lambda_1 = 1000$ and $\lambda_2 = 1$. The dimension of the set of basis functions is $\mathcal{N}^0 + \mathcal{N}^1 = 17$.

N	E: DPM2	Rate	E: DPM4	Rate
160	7.9331E-04	–	1.1962E-06	–
320	1.5312E-04	2.37	2.9307E-07	2.03
640	3.8833E-05	1.98	1.1668E-08	4.65
1280	9.3874E-06	2.05	6.6897E-10	4.12
N	E_{∇_x} : DPM2	Rate	E_{∇_x} : DPM4	Rate
160	1.8881E-03	–	3.9764E-06	–
320	4.5911E-04	2.04	1.0648E-06	1.90
640	1.4552E-04	1.66	3.5132E-08	4.92
1280	4.0391E-05	1.85	2.5000E-09	3.81
N	E_{∇_y} : DPM2	Rate	E_{∇_y} : DPM4	Rate
160	2.1015E-03	–	6.3942E-06	–
320	4.5735E-04	2.20	1.6593E-06	1.95
640	1.1380E-04	2.01	4.3716E-08	5.25
1280	3.1276E-05	1.86	2.2721E-09	4.27

Table 10

Grid convergence in the approximate solution and components of the discrete gradient for DPM2 (left) and DPM4 (right). The interior domain Ω_2 is the ellipse with $a = 1$, $b = 0.5$ centered at the origin, and the exterior domain is $\Omega_1 = [-2, 2] \times [-2, 2] \setminus \Omega_2$. Test problem (6.10), (6.11) with material coefficients $\lambda_1 = 1$ and $\lambda_2 = 1000$. The dimension of the set of basis functions is $\mathcal{N}^0 + \mathcal{N}^1 = 17$.

N	E: DPM2	Rate	E: DPM4	Rate
160	2.8834E-04	–	4.6351E-07	–
320	7.6116E-05	1.92	2.6459E-08	4.13
640	2.0678E-05	1.88	1.7726E-09	3.90
1280	4.9212E-06	2.07	1.0497E-10	4.08
N	E_{∇_x} : DPM2	Rate	E_{∇_x} : DPM4	Rate
160	5.5817E-04	–	6.7908E-07	–
320	1.5141E-04	1.88	4.4384E-08	3.94
640	4.5776E-05	1.73	2.8536E-09	3.96
1280	1.1892E-05	1.94	1.8616E-10	3.94
N	E_{∇_y} : DPM2	Rate	E_{∇_y} : DPM4	Rate
160	5.5629E-04	–	9.3938E-07	–
320	1.3835E-04	2.01	3.9553E-08	4.57
640	3.5578E-05	1.96	2.7175E-09	3.86
1280	9.3981E-06	1.92	1.7778E-10	3.93

Table 11

Grid convergence in the approximate solution and components of the discrete gradient for DPM2 (left) and DPM4 (right). The interior domain Ω_2 is the ellipse with $a = 0.9$, $b = 0.3$ centered at the origin, and the exterior domain is $\Omega_1 = [-2, 2] \times [-2, 2] \setminus \Omega_2$. Test problem (6.10), (6.11) with material coefficients $\lambda_1 = 1$ and $\lambda_2 = 1000$. The dimension of the set of basis functions is $\mathcal{N}^0 + \mathcal{N}^1 = 17$.

N	E: DPM2	Rate	E: DPM4	Rate
160	5.5513E-04	–	9.6244E-06	–
320	1.3776E-04	2.01	1.2031E-07	6.32
640	3.1185E-05	2.14	6.8993E-09	4.12
1280	7.5539E-06	2.05	4.1148E-10	4.07
N	E_{∇_x} : DPM2	Rate	E_{∇_x} : DPM4	Rate
160	1.2706E-03	–	2.8293E-05	–
320	3.9571E-04	1.68	2.4007E-07	6.88
640	1.1077E-04	1.84	1.8805E-08	3.67
1280	2.9727E-05	1.90	1.3124E-09	3.84
N	E_{∇_y} : DPM2	Rate	E_{∇_y} : DPM4	Rate
160	1.1064E-03	–	4.1055E-05	–
320	2.5858E-04	2.10	3.1522E-07	7.03
640	7.5354E-05	1.78	1.6035E-08	4.30
1280	2.0664E-05	1.87	1.0849E-09	3.89

Table 12

Grid convergence in the approximate solution and components of the discrete gradient for DPM2 (left) and DPM4 (right). The interior domain Ω_2 is the ellipse with $a = 1$, $b = 0.25$ centered at the origin, and the exterior domain is $\Omega_1 = [-2, 2] \times [-2, 2] \setminus \Omega_2$. Test problem (6.10), (6.11) with material coefficients $\lambda_1 = 1$ and $\lambda_2 = 1000$. The dimension of the set of basis functions is $\mathcal{N}^0 + \mathcal{N}^1 = 17$.

N	E: DPM2	Rate	E: DPM4	Rate
160	7.9331E-04	–	1.1962E-06	–
320	1.5312E-04	2.37	2.9307E-07	2.03
640	3.8833E-05	1.98	1.1668E-08	4.65
1280	9.3874E-06	2.05	6.6906E-10	4.12
N	E_{∇_x} : DPM2	Rate	E_{∇_x} : DPM4	Rate
160	1.8881E-03	–	3.9764E-06	–
320	4.5911E-04	2.04	1.0648E-06	1.90
640	1.4552E-04	1.66	3.5132E-08	4.92
1280	4.0391E-05	1.85	2.5001E-09	3.81
N	E_{∇_y} : DPM2	Rate	E_{∇_y} : DPM4	Rate
160	2.1015E-03	–	6.3942E-06	–
320	4.5735E-04	2.20	1.6593E-06	1.95
640	1.1380E-04	2.01	4.3716E-08	5.25
1280	3.1276E-05	1.86	2.2722E-09	4.27

Table 13

Grid convergence in the approximate solution and components of the discrete gradient for DPM2 (left) and DPM4 (right). The interior domain Ω_2 is the ellipse with $a = 1$, $b = 0.5$ centered at the origin, and the exterior domain is $\Omega_1 = [-2, 2] \times [-2, 2] \setminus \Omega_2$. Test problem (6.10), (6.12) with material coefficients $\lambda_1 = \lambda_2 = 1$. The dimension of the set of basis functions is $\mathcal{N}^0 + \mathcal{N}^1 = 44$.

N	E: DPM2	Rate	E: DPM4	Rate
160	2.8085E-02	–	1.4950E-03	–
320	7.2826E-03	1.95	9.7985E-05	3.93
640	1.8663E-03	1.96	6.1284E-06	4.00
1280	4.6748E-04	2.00	3.8400E-07	4.00
N	E_{∇_x} : DPM2	Rate	E_{∇_x} : DPM4	Rate
160	2.7484E-02	–	1.4435E-03	–
320	6.9980E-03	1.97	7.9235E-05	4.19
640	1.7454E-03	2.00	4.4775E-06	4.15
1280	4.3609E-04	2.00	2.7098E-07	4.05
N	E_{∇_y} : DPM2	Rate	E_{∇_y} : DPM4	Rate
160	2.2902E-02	–	9.5395E-04	–
320	5.8477E-03	1.97	5.9434E-05	4.00
640	1.7098E-03	1.77	3.6586E-06	4.02
1280	4.3067E-04	1.99	2.2893E-07	4.00

Table 14

Grid convergence in the approximate solution and components of the discrete gradient for DPM2 (left) and DPM4 (right). The interior domain Ω_2 is the ellipse with $a = 0.9$, $b = 0.3$ centered at the origin, and the exterior domain is $\Omega_1 = [-2, 2] \times [-2, 2] \setminus \Omega_2$. Test problem (6.10), (6.12) with material coefficients $\lambda_1 = \lambda_2 = 1$. The dimension of the set of basis functions is $\mathcal{N}^0 + \mathcal{N}^1 = 38$.

N	E: DPM2	Rate	E: DPM4	Rate
160	2.9284E-02	–	1.9136E-03	–
320	7.0108E-03	2.06	8.3014E-05	4.53
640	1.7471E-03	2.00	5.2579E-06	3.98
1280	4.3662E-04	2.00	3.2976E-07	4.00
N	E_{∇_x} : DPM2	Rate	E_{∇_x} : DPM4	Rate
160	2.7461E-02	–	1.7482E-03	–
320	6.9886E-03	1.97	7.9013E-05	4.47
640	1.7435E-03	2.00	4.4672E-06	4.14
1280	4.3568E-04	2.00	2.8587E-07	3.97
N	E_{∇_y} : DPM2	Rate	E_{∇_y} : DPM4	Rate
160	2.3129E-02	–	9.4881E-04	–
320	5.8410E-03	1.99	5.9249E-05	4.00
640	1.4562E-03	2.00	3.6146E-06	4.03
1280	3.6388E-04	2.00	2.2425E-07	4.01

Table 15

Grid convergence in the approximate solution and components of the discrete gradient for DPM2 (left) and DPM4 (right). The interior domain Ω_2 is the ellipse with $a = 1$, $b = 0.25$ centered at the origin, and the exterior domain is $\Omega_1 = [-2, 2] \times [-2, 2] \setminus \Omega_2$. Test problem (6.10), (6.12) with material coefficients $\lambda_1 = \lambda_2 = 1$. The dimension of the set of basis functions is $\mathcal{N}^0 + \mathcal{N}^1 = 39$.

N	E: DPM2	Rate	E: DPM4	Rate
160	3.5636E-02	–	1.9351E-03	–
320	8.3209E-03	2.10	1.0946E-04	4.14
640	2.0660E-03	2.01	6.7116E-06	4.03
1280	5.0977E-04	2.02	4.2396E-07	3.98
N	E_{∇_x} : DPM2	Rate	E_{∇_x} : DPM4	Rate
160	2.7462E-02	–	1.7184E-03	–
320	6.9932E-03	1.97	7.9082E-05	4.44
640	1.7448E-03	2.00	4.4704E-06	4.14
1280	4.3595E-04	2.00	2.7059E-07	4.05
N	E_{∇_y} : DPM2	Rate	E_{∇_y} : DPM4	Rate
160	2.3272E-02	–	9.5422E-04	–
320	5.8522E-03	1.99	5.9416E-05	4.01
640	1.6288E-03	1.85	3.6767E-06	4.01
1280	4.2909E-04	1.92	2.3031E-07	4.00

Table 16

Grid convergence in the approximate solution and components of the discrete gradient for DPM2 (left) and DPM4 (right). The interior domain Ω_2 is the ellipse with $a = 1$, $b = 0.5$ centered at the origin, and the exterior domain is $\Omega_1 = [-2, 2] \times [-2, 2] \setminus \Omega_2$. Test problem (6.10), (6.12) with material coefficients $\lambda_1 = 1000$ and $\lambda_2 = 1$. The dimension of the set of basis functions is $\mathcal{N}^0 + \mathcal{N}^1 = 44$.

N	E: DPM2	Rate	E: DPM4	Rate
160	2.8085E-02	–	1.4950E-03	–
320	7.2826E-03	1.95	9.7985E-05	3.93
640	1.8663E-03	1.96	6.1284E-06	4.00
1280	4.6748E-04	2.00	3.8400E-07	4.00
N	E_{∇_x} : DPM2	Rate	E_{∇_x} : DPM4	Rate
160	2.7484E-02	–	1.4435E-03	–
320	6.9980E-03	1.97	7.9235E-05	4.19
640	1.7454E-03	2.00	4.4775E-06	4.15
1280	4.3609E-04	2.00	2.7098E-07	4.05
N	E_{∇_y} : DPM2	Rate	E_{∇_y} : DPM4	Rate
160	2.2902E-02	–	9.5395E-04	–
320	5.8477E-03	1.97	5.9434E-05	4.00
640	1.7098E-03	1.77	3.6586E-06	4.02
1280	4.3067E-04	1.99	2.2893E-07	4.00

Table 17

Grid convergence in the approximate solution and components of the discrete gradient for DPM2 (left) and DPM4 (right). The interior domain Ω_2 is the ellipse with $a = 0.9$, $b = 0.3$ centered at the origin, and the exterior domain is $\Omega_1 = [-2, 2] \times [-2, 2] \setminus \Omega_2$. Test problem (6.10), (6.12) with material coefficients $\lambda_1 = 1000$ and $\lambda_2 = 1$. The dimension of the set of basis functions is $\mathcal{N}^0 + \mathcal{N}^1 = 38$.

N	E: DPM2	Rate	E: DPM4	Rate
160	2.9284E-02	–	1.9136E-03	–
320	7.0108E-03	2.06	8.3014E-05	4.53
640	1.7471E-03	2.00	5.2579E-06	3.98
1280	4.3662E-04	2.00	3.2976E-07	4.00
N	E_{∇_x} : DPM2	Rate	E_{∇_x} : DPM4	Rate
160	2.7461E-02	–	1.7482E-03	–
320	6.9886E-03	1.97	7.9013E-05	4.47
640	1.7435E-03	2.00	4.4672E-06	4.14
1280	4.3568E-04	2.00	2.8587E-07	3.97
N	E_{∇_y} : DPM2	Rate	E_{∇_y} : DPM4	Rate
160	2.3129E-02	–	9.4881E-04	–
320	5.8410E-03	1.99	5.9249E-05	4.00
640	1.4562E-03	2.00	3.6146E-06	4.03
1280	3.6388E-04	2.00	2.2425E-07	4.01

Table 18

Grid convergence in the approximate solution and components of the discrete gradient for DPM2 (left) and DPM4 (right). The interior domain Ω_2 is the ellipse with $a = 1$, $b = 0.25$ centered at the origin, and the exterior domain is $\Omega_1 = [-2, 2] \times [-2, 2] \setminus \Omega_2$. Test problem (6.10), (6.12) with material coefficients $\lambda_1 = 1000$ and $\lambda_2 = 1$. The dimension of the set of basis functions is $\mathcal{N}^0 + \mathcal{N}^1 = 39$.

N	E: DPM2	Rate	E: DPM4	Rate
160	3.5636E-02	–	1.9351E-03	–
320	8.3209E-03	2.10	1.0946E-04	4.14
640	2.0660E-03	2.01	6.7116E-06	4.03
1280	5.0977E-04	2.02	4.2396E-07	3.98
N	E_{∇_x} : DPM2	Rate	E_{∇_x} : DPM4	Rate
160	2.7462E-02	–	1.7184E-03	–
320	6.9932E-03	1.97	7.9082E-05	4.44
640	1.7448E-03	2.00	4.4704E-06	4.14
1280	4.3595E-04	2.00	2.7059E-07	4.05
N	E_{∇_y} : DPM2	Rate	E_{∇_y} : DPM4	Rate
160	2.3272E-02	–	9.5422E-04	–
320	5.8522E-03	1.99	5.9416E-05	4.01
640	1.6288E-03	1.85	3.6767E-06	4.01
1280	4.2909E-04	1.92	2.3031E-07	4.00

Table 19

Grid convergence in the approximate solution and components of the discrete gradient for DPM2 (left) and DPM4 (right). The interior domain Ω_2 is the ellipse with $a = 1$, $b = 0.5$ centered at the origin, and the exterior domain is $\Omega_1 = [-2, 2] \times [-2, 2] \setminus \Omega_2$. Test problem (6.10), (6.12) with material coefficients $\lambda_1 = 1$ and $\lambda_2 = 1000$. The dimension of the set of basis functions is $\mathcal{N}^0 + \mathcal{N}^1 = 44$.

N	E: DPM2	Rate	E: DPM4	Rate
160	2.8085E-02	–	1.4950E-03	–
320	7.2826E-03	1.95	9.7985E-05	3.93
640	1.8663E-03	1.96	6.1284E-06	4.00
1280	4.6748E-04	2.00	3.8400E-07	4.00
N	E_{∇_x} : DPM2	Rate	E_{∇_x} : DPM4	Rate
160	2.7484E-02	–	1.4435E-03	–
320	6.9980E-03	1.97	7.9235E-05	4.19
640	1.7454E-03	2.00	4.4775E-06	4.15
1280	4.3609E-04	2.00	2.7098E-07	4.05
N	E_{∇_y} : DPM2	Rate	E_{∇_y} : DPM4	Rate
160	2.2902E-02	–	9.5395E-04	–
320	5.8477E-03	1.97	5.9434E-05	4.00
640	1.7098E-03	1.77	3.6586E-06	4.02
1280	4.3067E-04	1.99	2.2893E-07	4.00

Table 20

Grid convergence in the approximate solution and components of the discrete gradient for DPM2 (left) and DPM4 (right). The interior domain Ω_2 is the ellipse with $a = 0.9$, $b = 0.3$ centered at the origin, and the exterior domain is $\Omega_1 = [-2, 2] \times [-2, 2] \setminus \Omega_2$. Test problem (6.10), (6.12) with material coefficients $\lambda_1 = 1$ and $\lambda_2 = 1000$. The dimension of the set of basis functions is $\mathcal{N}^0 + \mathcal{N}^1 = 38$.

N	E: DPM2	Rate	E: DPM4	Rate
160	2.9284E-02	–	1.9136E-03	–
320	7.0108E-03	2.06	8.3014E-05	4.53
640	1.7471E-03	2.00	5.2579E-06	3.98
1280	4.3662E-04	2.00	3.2976E-07	4.00
N	E_{∇_x} : DPM2	Rate	E_{∇_x} : DPM4	Rate
160	2.7461E-02	–	1.7482E-03	–
320	6.9886E-03	1.97	7.9013E-05	4.47
640	1.7435E-03	2.00	4.4672E-06	4.14
1280	4.3568E-04	2.00	2.8587E-07	3.97
N	E_{∇_y} : DPM2	Rate	E_{∇_y} : DPM4	Rate
160	2.3129E-02	–	9.4881E-04	–
320	5.8410E-03	1.99	5.9249E-05	4.00
640	1.4562E-03	2.00	3.6146E-06	4.03
1280	3.6388E-04	2.00	2.2425E-07	4.01

Table 21

Grid convergence in the approximate solution and components of the discrete gradient for DPM2 (left) and DPM4 (right). The interior domain Ω_2 is the ellipse with $a = 1$, $b = 0.25$ centered at the origin, and the exterior domain is $\Omega_1 = [-2, 2] \times [-2, 2] \setminus \Omega_2$. Test problem (6.10), (6.12) with material coefficients $\lambda_1 = 1$ and $\lambda_2 = 1000$. The dimension of the set of basis functions is $\mathcal{N}^0 + \mathcal{N}^1 = 39$.

N	E: DPM2	Rate	E: DPM4	Rate
160	3.5636E-02	–	1.9351E-03	–
320	8.3209E-03	2.10	1.0946E-04	4.14
640	2.0660E-03	2.01	6.7116E-06	4.03
1280	5.0977E-04	2.02	4.2396E-07	3.98
N	E_{∇_x} : DPM2	Rate	E_{∇_x} : DPM4	Rate
160	2.7462E-02	–	1.7184E-03	–
320	6.9932E-03	1.97	7.9082E-05	4.44
640	1.7448E-03	2.00	4.4704E-06	4.14
1280	4.3595E-04	2.00	2.7059E-07	4.05
N	E_{∇_y} : DPM2	Rate	E_{∇_y} : DPM4	Rate
160	2.3272E-02	–	9.5422E-04	–
320	5.8522E-03	1.99	5.9416E-05	4.01
640	1.6288E-03	1.85	3.6767E-06	4.01
1280	4.2909E-04	1.92	2.3031E-07	4.00

Table 22

Grid convergence in the approximate solution and components of the discrete gradient for DPM2 (left) and DPM4 (right) using *non-matching grids*. The interior domain Ω_2 is the ellipse with $a = 1$, $b = 0.5$ centered at the origin, and the exterior domain is $\Omega_1 = [-2, 2] \times [-2, 2] \setminus \Omega_2$. Test problem (6.10), (6.12) with material coefficients $\lambda_1 = 1$ and $\lambda_2 = 1$. The dimension of the set of basis functions is $\mathcal{N}^0 + \mathcal{N}^1 = 58$.

N_1	N_2	E: DPM2	Rate	E: DPM4	Rate
160	40	9.4441E-02	–	2.1790E-03	–
320	80	7.6122E-03	3.63	9.7015E-05	4.49
640	160	1.8695E-03	2.03	6.1537E-06	3.98
1280	320	4.6884E-04	2.00	3.8517E-07	4.00
N_1	N_2	E_{∇_x} : DPM2	Rate	E_{∇_x} : DPM4	Rate
160	40	1.2899E-01	–	1.4478E-03	–
320	80	7.0014E-03	4.20	7.9228E-05	4.19
640	160	1.7454E-03	2.00	4.4775E-06	4.15
1280	320	4.3608E-04	2.00	2.7098E-07	4.05
N_1	N_2	E_{∇_y} : DPM2	Rate	E_{∇_y} : DPM4	Rate
160	40	4.8685E-02	–	9.6113E-04	–
320	80	5.8527E-03	3.06	5.9424E-05	4.02
640	160	1.7078E-03	1.78	3.6596E-06	4.02
1280	320	4.3147E-04	1.98	2.2897E-07	4.00

Table 23

Grid convergence in the approximate solution and components of the discrete gradient for DPM2 (left) and DPM4 (right) (using the same grids for domain Ω_1 and Ω_2). The interior domain Ω_2 is the ellipse with $a = 1$, $b = 0.5$ centered at the origin, and the exterior domain is $\Omega_1 = [-2, 2] \times [-2, 2] \setminus \Omega_2$. Test problem (6.10), (6.12) with material coefficients $\lambda_1 = 1$ and $\lambda_2 = 1$. The dimension of the set of basis functions is $\mathcal{N}^0 + \mathcal{N}^1 = 58$.

N	E: DPM2	Rate	E: DPM4	Rate
160	2.8082E-02	–	1.4974E-03	–
320	7.2795E-03	1.95	9.7989E-05	3.93
640	1.8656E-03	1.96	6.1285E-06	4.00
1280	4.6731E-04	2.00	3.8400E-07	4.00
N	E_{∇_x} : DPM2	Rate	E_{∇_x} : DPM4	Rate
160	2.7484E-02	–	1.4435E-03	–
320	6.9980E-03	1.97	7.9235E-05	4.19
640	1.7454E-03	2.00	4.4775E-06	4.15
1280	4.3609E-04	2.00	2.7098E-07	4.05
N	E_{∇_y} : DPM2	Rate	E_{∇_y} : DPM4	Rate
160	2.2902E-02	–	9.5397E-04	–
320	5.8477E-03	1.97	5.9435E-05	4.00
640	1.7061E-03	1.78	3.6586E-06	4.02
1280	4.3069E-04	1.99	2.2893E-07	4.00

Table 24

Grid convergence in the approximate solution using *mixed-order* DPM (Ω_1 is the fourth-order and Ω_2 is the second-order). The interior domain Ω_2 is the ellipse with $a = 1$, $b = 0.5$ centered at the origin, and the exterior domain is $\Omega_1 = [-2, 2] \times [-2, 2] \setminus \Omega_2$. Test problem (6.10), (6.12) with material coefficients $\lambda_1 = 1$ and $\lambda_2 = 1$. The dimension of the set of basis functions is $\mathcal{N}^0 + \mathcal{N}^1 = 61$.

N	E: DPM	Rate
160	1.5116E-03	–
320	1.0125E-04	3.90
640	1.1996E-05	3.08
1280	2.6518E-06	2.18

Again, we employ for DPM the following auxiliary domains in Tables 22–26:

$$\Omega_1^0 \equiv \Omega_2^0 = [-2, 2] \times [-2, 2].$$

6.4. Second-order (DPM2) and fourth-order (DPM4): example of application

In this section we illustrate robustness of the developed methods by considering the linear static model of biological cell electropermeabilization which arises in Biological/Biomedical applications. The model under consideration (6.13)–(6.16)

Table 25
Corresponding errors in the discrete gradient using mixed-order DPM.

N	$E_{\nabla x}$	Rate	$E_{\nabla y}$	Rate
160	1.4435E-03	–	9.5438E-04	–
320	7.9236E-05	4.19	5.9534E-05	4.00
640	8.3207E-06	3.25	3.6849E-06	4.01
1280	1.6819E-06	2.31	3.5632E-07	3.37

Table 26
Grid convergence in the approximate solution and components of the discrete gradient for DPM2 (left) and DPM4 (right). The interior domain Ω_2 is the ellipse with $a = 1$, $b = 0.5$ centered at the origin, and the exterior domain is $\Omega_1 = [-2, 2] \times [-2, 2] \setminus \Omega_2$. Test problem (6.10), (6.12) with material coefficients $\lambda_1 = 1$ and $\lambda_2 = 1$. The dimension of the set of basis functions is $\mathcal{N}^0 + \mathcal{N}^1 = 61$.

N	E: DPM2	Rate	E: DPM4	Rate
160	2.8076E-02	–	1.4976E-03	–
320	7.2801E-03	1.95	9.7989E-05	3.93
640	1.8656E-03	1.96	6.1285E-06	4.00
1280	4.6731E-04	2.00	3.8400E-07	4.00

N	$E_{\nabla x}$: DPM2	Rate	$E_{\nabla x}$: DPM4	Rate
160	2.7484E-02	–	1.4435E-03	–
320	6.9980E-03	1.97	7.9235E-05	4.19
640	1.7454E-03	2.00	4.4775E-06	4.15
1280	4.3609E-04	2.00	2.7098E-07	4.05

N	$E_{\nabla y}$: DPM2	Rate	$E_{\nabla y}$: DPM4	Rate
160	2.2902E-02	–	9.5398E-04	–
320	5.8477E-03	1.97	5.9435E-05	4.00
640	1.7061E-03	1.78	3.6586E-06	4.02
1280	4.3068E-04	1.99	2.2893E-07	4.00

is the elliptic interface model. This model describes the induced transmembrane voltage of a biological cell in an external electric field. If a cell is exposed to a sufficiently strong electric field, then this produces a strong increase in membrane permeability. As a consequence, molecules for which the membrane was impermeable can be transported across the membrane. This phenomenon (known as the electroporation or electropermeabilization) has many applications in biochemistry, molecular biology, and medicine, for example in oncology (electrochemotherapy of tumors), see [27].

We consider here a linear static model (6.13)–(6.16) where the electric potentials in both domains do not depend on time (see [27] and [14]). The equations (6.13) are subject to interface (6.14)–(6.15) and Dirichlet boundary conditions (6.16):

$$\nabla \cdot (\lambda_s \nabla V_s) = 0, \quad s \in \{1, 2\} \tag{6.13}$$

$$V_1|_{\Gamma} - V_2|_{\Gamma} = \frac{\lambda_2}{S_L} \frac{\partial V_2}{\partial n} \Big|_{\Gamma}, \tag{6.14}$$

$$\lambda_1 \frac{\partial V_1}{\partial n} \Big|_{\Gamma} - \lambda_2 \frac{\partial V_2}{\partial n} \Big|_{\Gamma} = 0, \tag{6.15}$$

$$V|_{\partial\Omega_1} = V_1|_{\partial\Omega_1}, \tag{6.16}$$

where V_s are the electric potentials, λ_s are the conductivities, ($s = 1, 2$), n is the outward normal vector, and S_L is the membrane surface conductivity. The Dirichlet boundary condition (6.16) is given by the analytic solution (6.17)–(6.18) (see [14]) at the boundary $\partial\Omega_1$ of the computational domain (i.e. auxiliary domain), see Fig. 8:

$$V_1(r, \theta) = \left(\alpha_1 r + \frac{\beta_1}{r} \right) \cos \theta, \quad R_1 < r < R_2, \tag{6.17}$$

$$V_2(r, \theta) = \alpha_2 r \cos \theta, \quad r < R_1. \tag{6.18}$$

Here, the constants are defined as

$$\alpha_2 = - \left(\left(\frac{\lambda_2}{S_L R_1} + 1 + \frac{\lambda_2}{\lambda_1} \right) R_2 + \left(\frac{\lambda_2}{S_L R_1} + 1 - \frac{\lambda_2}{\lambda_1} \right) \frac{R_1^2}{R_2} \right)^{-1} E_a R_2.$$

$$\alpha_1 = \frac{1}{2} \left(\frac{\lambda_2}{S_L R_1} + 1 + \frac{\lambda_2}{\lambda_1} \right) \alpha_2.$$

$$\beta_1 = \frac{1}{2} \left(\frac{\lambda_2}{S_L R_1} + 1 - \frac{\lambda_2}{\lambda_1} \right) \alpha_2 R_1^2.$$

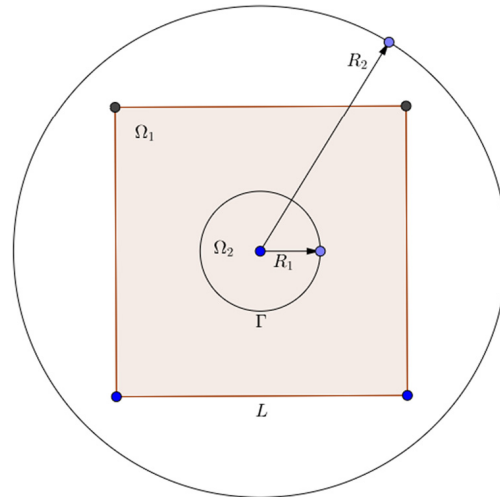


Fig. 8. Domains of calculation of the analytical and numerical solutions: analytical solution is computed inside of the circle with radius R_2 . Circle with radius R_1 is the cell. Analytical solution at the boundary of the computational domain Ω_1 (square with edge L) gives the Dirichlet boundary condition for the numerical simulation.

Table 27
Model parameters for analytical solution and numerical simulation.

Variable	Symbol	Value	Unit
Extracellular conductivity	λ_1	5	S/m
Intracellular conductivity	λ_2	0.455	S/m
Membrane surface conductivity	S_L	1.9	S/m ²
Cell radius	R_1	50	μm
Analytic solution domain radius	R_2	150	μm
Electric field magnitude	E_a	400	V/cm
Edge of computational domain	L	200	μm

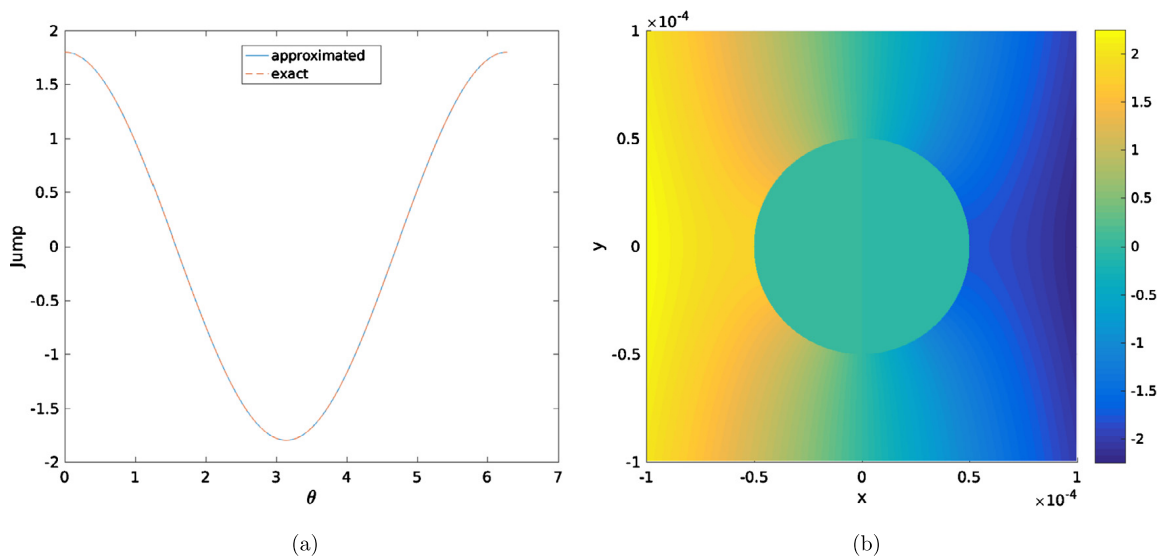


Fig. 9. (a) Comparison of analytical jump and numerical jump over the circle with respect to angle; (b) Numerical solution in Ω_1 and Ω_2 .

Above, θ is the corresponding angle at the interface (degenerated membrane), and E_a is the electric field magnitude (the electric field is in the positive direction of the x -axis). Parameters in Table 27 are used for both analytical and numerical simulation, and are employed from [14].

The difference of the electric potentials (6.14) between cell interior and exterior is explicitly given and draws interest to researchers, see [27]. We compared the jump from the numerical simulation with the analytical one, and we observed an excellent agreement. Furthermore, from the numerical solution we clearly see that the cell is polarized, see Fig. 9.

Table 28

Grid convergence in the approximate solution and components of the discrete gradient for DPM2 (left) and DPM4 (right). The interior domain Ω_2 is the circle with $R_1 = 5 \times 10^{-5}$ m centered at the origin, and the exterior domain is $\Omega_1 = [-10^{-4}, 10^{-4}] \times [-10^{-4}, 10^{-4}] \setminus \Omega_2$. Electroporation model problem (6.13)–(6.16) with material coefficients $\lambda_1 = 5$ and $\lambda_2 = 0.455$. The dimension of the set of basis functions is $\mathcal{N}^0 + \mathcal{N}^1 = 2$.

N	E: DPM2	Rate	E: DPM4	Rate
160	7.9569E–05	–	9.2776E–08	–
320	2.0603E–05	1.95	6.3054E–09	3.88
640	4.9672E–06	2.05	3.8796E–10	4.02
1280	1.2117E–06	2.04	2.1193E–11	4.19
N	E_{∇_x} : DPM2	Rate	E_{∇_x} : DPM4	Rate
160	2.8232E–04	–	1.9647E–07	–
320	7.2623E–05	1.96	1.3254E–08	3.89
640	1.8210E–05	2.00	8.5474E–10	3.95
1280	4.5676E–06	2.00	6.1582E–11	3.79
N	E_{∇_y} : DPM2	Rate	E_{∇_y} : DPM4	Rate
160	2.9191E–04	–	2.5434E–07	–
320	8.4842E–05	1.78	1.6466E–08	3.95
640	2.1394E–05	1.99	1.0334E–09	3.99
1280	5.2856E–06	2.02	8.3343E–11	3.63

We computed the numerical solution along with the discrete gradient using both DPM2 and DPM4. Second-order and fourth-order accuracy are recovered in both the solution and the discrete gradient, see Table 28.

7. Conclusion

In this paper, we developed efficient high-order accurate methods based on Difference Potentials for 2D elliptic models with material interfaces. We presented the construction of Difference Potentials Methods with high-order accuracy for single domain, and for the interface/composite domain problems with non-matching interface conditions. The numerical discretization (for example, numerical methods with different orders of the approximation in different subdomains/domains), as well as meshes can be chosen totally independently for each subdomain/domain and the boundaries of the subdomains/interfaces do not need to conform/align with the grids. The constructed numerical algorithms are not restricted by the choice of boundary conditions, and the main computational complexity of the designed algorithms reduces to the several solutions of simple auxiliary problems on regular structured grids. Moreover, 2D numerical experiments clearly illustrate the capability of Difference Potentials approach to resolve discontinuities with high-order accuracy at the material interfaces.

For near future research, we plan to develop p - and h -adaptive algorithms based on the Difference Potentials approach (including we plan to investigate optimal basis to represent traces at the boundary/interface), as well as extend methods here and in [2] to models in heterogeneous media in 2D and 3D domains.

Acknowledgement

The research of Jason Albright, Yekaterina Epshteyn and Qing Xia is supported in part by the National Science Foundation Grant # DMS-1112984.

References

- [1] J. Albright, Y. Epshteyn, K.R. Steffen, High-order accurate difference potentials methods for parabolic problems, *Appl. Numer. Math.* 93 (2015) 87–106, <http://dx.doi.org/10.1016/j.apnum.2014.08.002>.
- [2] J. Albright, Y. Epshteyn, Q. Xia, High-order accurate methods based on difference potentials for 2D parabolic interface models, submitted for publication, 2015.
- [3] I. Babuška, The finite element method for elliptic equations with discontinuous coefficients, *Computing (Arch. Elektron. Rechnen)* 5 (1970) 207–213.
- [4] J.T. Beale, A.T. Layton, On the accuracy of finite difference methods for elliptic problems with interfaces, *Commun. Appl. Math. Comput. Sci.* 1 (2006) 91–119, <http://dx.doi.org/10.2140/camcos.2006.1.91> (electronic).
- [5] D. Britt, S. Tsynkov, E. Turkel, A high-order numerical method for the Helmholtz equation with nonstandard boundary conditions, *SIAM J. Sci. Comput.* 35 (5) (2013) A2255–A2292, <http://epubs.siam.org/doi/abs/10.1137/120902689>.
- [6] Z. Chen, J. Zou, Finite element methods and their convergence for elliptic and parabolic interface problems, *Numer. Math.* 79 (2) (1998) 175–202, <http://dx.doi.org/10.1007/s002110050336>.
- [7] Y. Epshteyn, Upwind-difference potentials method for Patlak–Keller–Segel chemotaxis model, *J. Sci. Comput.* 53 (3) (2012) 689–713.
- [8] Y. Epshteyn, Algorithms composition approach based on difference potentials method for parabolic problems, *Commun. Math. Sci.* 12 (4) (2014) 723–755.
- [9] Y. Epshteyn, M. Medvinsky, On the solution of the elliptic interface problems by difference potentials method, in: *Lect. Notes Comput. Sci. Eng.*, vol. 106, 2015, pp. 197–205.
- [10] Y. Epshteyn, S. Phippen, High-order difference potentials methods for 1D elliptic type models, *Appl. Numer. Math.* 93 (July 2015) 69–86, <http://dx.doi.org/10.1016/j.apnum.2014.02.005>.

- [11] Y. Epshteyn, I. Sofronov, S. Tsynkov, Professor V.S. Ryaben'kii. On the occasion of the 90-th birthday [Editorial], *Appl. Numer. Math.* 93 (2015) 1–2, <http://dx.doi.org/10.1016/j.apnum.2015.02.001>.
- [12] R.P. Fedkiw, T. Aslam, B. Merriman, S. Osher, A non-oscillatory Eulerian approach to interfaces in multimaterial flows (the ghost fluid method), *J. Comput. Phys.* 152 (2) (1999) 457–492, <http://dx.doi.org/10.1006/jcph.1999.6236>.
- [13] J. Guzman, M. Sanchez, M. Sarkis, On the accuracy of finite element approximations to a class of interface problems, *Math. Comput.* 85 (301) (2016) 2071–2098.
- [14] O. Kavian, M. Leguèbe, C. Poinard, L. Weynans, Classical electroporation modeling at the cell scale, *J. Math. Biol.* 68 (1–2) (2014) 235–265.
- [15] R.J. LeVeque, Z.L. Li, The immersed interface method for elliptic equations with discontinuous coefficients and singular sources, *SIAM J. Numer. Anal.* 31 (4) (1994) 1019–1044, <http://dx.doi.org/10.1137/0731054>.
- [16] R.J. LeVeque, Z. Li, Immersed interface methods for Stokes flow with elastic boundaries or surface tension, *SIAM J. Sci. Comput.* 18 (3) (1997) 709–735, <http://dx.doi.org/10.1137/S1064827595282532>.
- [17] Z. Li, K. Ito, The immersed interface method, in: *Numerical Solutions of PDEs Involving Interfaces and Irregular Domains*, in: *Front. Math. Appl.*, vol. 33, Society for Industrial and Applied Mathematics (SIAM), Philadelphia, PA, 2006.
- [18] X.-D. Liu, T.C. Sideris, Convergence of the ghost fluid method for elliptic equations with interfaces, *Math. Comput.* 72 (244) (2003) 1731–1746, <http://dx.doi.org/10.1090/S0025-5718-03-01525-4> (electronic).
- [19] X.-D. Liu, R.P. Fedkiw, M. Kang, A boundary condition capturing method for Poisson's equation on irregular domains, *J. Comput. Phys.* 160 (1) (2000) 151–178, <http://dx.doi.org/10.1006/jcph.2000.6444>.
- [20] J. Loncaric, V.S. Ryaben'kii, S.V. Tsynkov, Active shielding and control of noise, *SIAM J. Appl. Math.* 62 (2) (2001) 563–596 (electronic).
- [21] A. Mayo, The fast solution of Poisson's and the biharmonic equations on irregular regions, *SIAM J. Numer. Anal.* 21 (2) (1984) 285–299, <http://dx.doi.org/10.1137/0721021>.
- [22] M. Medvinsky, S. Tsynkov, E. Turkel, The method of difference potentials for the Helmholtz equation using compact high order schemes, *J. Sci. Comput.* 53 (1) (2012) 150–193.
- [23] M. Medvinsky, S. Tsynkov, E. Turkel, High order numerical simulation of the transmission and scattering of waves using the method of difference potentials, *J. Comput. Phys.* 243 (2013) 305–322, <http://dx.doi.org/10.1016/j.jcp.2013.03.014>.
- [24] L. Mu, J. Wang, G. Wei, X. Ye, S. Zhao, Weak Galerkin methods for second order elliptic interface problems, *J. Comput. Phys.* 250 (2013) 106–125, <http://www.sciencedirect.com/science/article/pii/S0021999113003367>.
- [25] C.S. Peskin, Numerical analysis of blood flow in the heart, *J. Comput. Phys.* 25 (3) (1977) 220–252.
- [26] C.S. Peskin, The immersed boundary method, *Acta Numer.* 11 (2002) 479–517, <http://dx.doi.org/10.1017/S0962492902000077>.
- [27] G. Pucihar, T. Kotnik, B. Valič, D. Miklavčič, Numerical determination of transmembrane voltage induced on irregularly shaped cells, *Ann. Biomed. Eng.* 34 (4) (2006) 642–652.
- [28] A.A. Reznik, Approximation of surface potentials of elliptic operators by difference potentials, *Dokl. Akad. Nauk SSSR* 263 (6) (1982) 1318–1321.
- [29] A.A. Reznik, Approximation of surface potentials of elliptic operators by difference potentials and solution of boundary value problems, Ph.D., Moscow, MPTI.
- [30] V.S. Ryaben'kii, Boundary equations with projectors, *Usp. Mat. Nauk* 40 (2 (242)) (1985) 121–149, 238.
- [31] V.S. Ryaben'kii, *Method of Difference Potentials and Its Applications*, Springer Ser. Comput. Math., vol. 30, Springer-Verlag, Berlin, 2002.
- [32] V.S. Ryaben'kii, Difference potentials analogous to Cauchy integrals, *Usp. Mat. Nauk* 67 (3 (405)) (2012) 147–172.
- [33] V.S. Ryaben'kii, S.V. Tsynkov, Artificial boundary conditions for the numerical solution of external viscous flow problems, *SIAM J. Numer. Anal.* 32 (5) (1995) 1355–1389.
- [34] V. Ryaben'kii, V.I. Turchaninov, Y.Y. Epshteyn, The numerical example of algorithms composition for solution of the boundary-value problems on compound domain based on difference potential method, Moscow, Keldysh Institute for Applied Mathematics, Russia Academy of Sciences (3).
- [35] V.S. Ryaben'kii, V.I. Turchaninov, E.Y. Ėpshteĭn, An algorithm composition scheme for problems in composite domains based on the method of difference potentials, *Zh. Vychisl. Mat. Mat. Fiz.* 10 (2006) 1853–1870.
- [36] V.S. Ryaben'kii, S.V. Tsynkov, S.V. Utyuzhnikov, Active control of sound with variable degree of cancellation, *Appl. Math. Lett.* 22 (12) (2009) 1846–1851, <http://dx.doi.org/10.1016/j.aml.2009.07.010>.
- [37] R.K. Sinha, B. Deka, Optimal error estimates for linear parabolic problems with discontinuous coefficients, *SIAM J. Numer. Anal.* 43 (2) (2005) 733–749, <http://dx.doi.org/10.1137/040605357> (electronic).
- [38] E. Tadmor, A review of numerical methods for nonlinear partial differential equations, *Bull. Am. Math. Soc. (N.S.)* 49 (4) (2012) 507–554, <http://dx.doi.org/10.1090/S0273-0979-2012-01379-4>.
- [39] S. Tsynkov, Numerical solution of problems on unbounded domains. A review, in: *Absorbing Boundary Conditions*, *Appl. Numer. Math.* 27 (4) (1998) 465–532.
- [40] S.V. Utyuzhnikov, Generalized Calderón–Ryaben'kii's potentials, *IMA J. Appl. Math.* 74 (1) (2009) 128–148, <http://dx.doi.org/10.1093/imamat/hxn025>.
- [41] S.V. Utyuzhnikov, Nonlinear problem of active sound control, *J. Comput. Appl. Math.* 234 (1) (2010) 215–223, <http://dx.doi.org/10.1016/j.cam.2009.12.017>.
- [42] E. Wadbro, S. Zahedi, G. Kreiss, M. Berggren, A uniformly well-conditioned, unfitted Nitsche method for interface problems: Part II, in preparation.
- [43] S. Yu, Y. Zhou, G.W. Wei, Matched interface and boundary (MIB) method for elliptic problems with sharp-edged interfaces, *J. Comput. Phys.* 224 (2) (2007) 729–756, <http://dx.doi.org/10.1016/j.jcp.2006.10.030>.
- [44] S. Zahedi, E. Wadbro, G. Kreiss, M. Berggren, A uniformly well-conditioned, unfitted Nitsche method for interface problems: Part I, in preparation.
- [45] Y.C. Zhou, S. Zhao, M. Feig, G.W. Wei, High order matched interface and boundary method for elliptic equations with discontinuous coefficients and singular sources, *J. Comput. Phys.* 213 (1) (2006) 1–30, <http://dx.doi.org/10.1016/j.jcp.2005.07.022>.
- [46] Y.C. Zhou, J. Liu, D.L. Harry, A matched interface and boundary method for solving multi-flow Navier–Stokes equations with applications to geodynamics, *J. Comput. Phys.* 231 (1) (2012) 223–242, <http://dx.doi.org/10.1016/j.jcp.2011.09.010>.